A Study of Incomplete Fusion Reaction and its Correlation with Projectile Energy and Entrance channel Mass-Asymmetry in some $^{12}C/^{16}O$-Induced Reactions at ≈3–9 MeV/nucleon

By, Mustefa Kedir Dubiso

M.Sc. Thesis Submitted to Hawassa University Department of Physics, College of Natural and Computational Science, School of Graduate Studies, Hawassa University, Hawassa Ethiopia

In Partial Fulfilment of the Requirements for the Degree of Master of science in Physics

(Nuclear Physics)

Hawassa, Ethiopia

May, 2024

SCHOOL OF GRADUATE STUDIES

HAWASSA UNIVERSITY

ADVISOR'S APPROVAL SHEET

This is to certify that the thesis entitled "**A study of incomplete fusion reaction and its correlation with projectile energy and entrance channel mass-asymmetry in some ^{12}C/^{16}O-induced reactions at ≈3–9 MeV/nucleon**" submitted in partial fulfilment of the requirements for the degree of Masters of science in physics with specialization in Nuclear physics, the graduate program of the Department of Physics, and has been carried out by Mustefa Kedir Id. No GpPhyR/0008/15, under my supervision. Therefore I recommend that the student has fulfilled the requirements and hence hereby can submit the thesis to the department.

Dr. Amanuel Fessahatsion	______________	______________
Advisor	signature	Date

HAWASSA UNIVERSITY

SCHOOLS OF GRADUATE STUDIES

EXAMINER'S APPROVAL SHEET

We, the undersigned, members of the broad of examiners of the final open defense by Mustefa Kedir have read and evaluated his thesis in entitled "**A Study of Incomplete Fusion Reaction and its Correlation With Projectile Energy and Entrance Channel Mass-Asymmetry in some 12C/16O-Induced Reaction at ≈ 3-9 MeV/nucleon''** and examined the candidate. This is therefore to certify that the thesis has been accepted in partial fulfillment of the requirement for the degree of Masters in Physics.

______________________	________________	_______________
Name of Major Advisor	Signature	Date
______________________	________________	_______________
Name of Internal Examiner- I	Signature	Date
______________________	________________	_______________
Name of Internal Examiner -II	Signature	Date
______________________	________________	_______________
Name of External Examiner	Signature	Date
______________________	________________	_______________
SGS Approval	Signature	Date

Finally approval and acceptance of the thesis is contingent up on the submission of the finally copy of the thesis to the school of Graduate studies (SGS) through the Department/School graduate committee (DGC/SGS) of the candidate's department.

Stamp of SGS Date: _______________

Declaration

I hereby declare that this MSc Thesis is my original work and has not been presented for a degree in any other university and that all sources of material used for the thesis have been duly acknowledged.

Name: Mustefa Kedir

Signature: ____________

This MSc thesis has been submitted for examination with my approval as university advisor.

Name: Dr. Amanuel Fissehatsion

Signature: ______________

Place and date of submission

Acknowledgments

I would like to express my deepest and sincere gratitude to my advisor Dr. F.K.Amanuel for his valuable assistance, guidance, supervision, patience with all my questions, suggestions and for his valuable comments on this thesis.

Besides I thanks to Hawassa University (Department of Physics) for the financial support provided and for extending facilities for performing this thesis.

Abstract

In this work, the effects of projectile energy and entrance channel mass-asymmetry on incomplete fusion reaction in ^{12}C + ^{128}Te, ^{12}C + ^{141}Pr, ^{12}C + ^{159}Tb, ^{16}O + ^{130}Te, ^{16}O + ^{159}Tb and ^{16}O + ^{181}Ta, projectiles + targets systems at ≈ 3-9 MeV/nucleon were studied. Cross sections of various reaction products populated via complete and incomplete fusion of ^{12}C projectile with ^{128}Te, ^{141}Pr and ^{159}Tb-targets and ^{16}O projectile with ^{130}Te, ^{159}Tb and ^{181}Ta targets were calculated using the reaction model code PACE4. The predicted cross sections were compared with experimentally measured data from EXFOR database. For a representative non α-emitting (^{12}C, 4n) channel from a representative in ^{12}C + ^{159}Tb system, experimentally measured cross sections agreed with PACE4 prediction for level density parameters K=10. For the same level density parameters a representative α-emitting (^{12}C, α3n) from a representative in ^{12}C + ^{128}Te projectile + target system, the experimentally measured cross sections are higher than the PACE4 predicted. The observed difference is attributed to the contribution of incomplete fusion following the prompt break-up of the projectiles into α-clusters. An attempt was made to deduce the contribution of incomplete fusion reactions from presently investigated projectile and target systems. It was found that the incomplete fusion fraction, in general, increases with the increase in projectile energy. Furthermore, the result indicated that at the same normalized relative velocity, the incomplete fusion fraction is higher for mass-asymmetric projectiles and targets systems.

Abbreviations

ICF: Incomplete Fusion

CF: Complete Fusion

V_{CB}: Energy Coulomb Barriers

BUF: Break-up Fusion

PEP: Promptly Emitted Particles

MSD: Multi-step Direct

σ_{ICF} $(total)$: Total incomplete fusion cross sections

E_{lab}: Energy of Laboratory

F_{ICF}: Incomplete fusion fraction

v_{rel}: Relative velocity

A_p: Projectile mass number

A_T: target mass number

CN: compound nucleus

Contents

List of figures

CHAPTER ONE

1. INTRODUCTION

For the past few decades, several efforts have been put forward by both experimental as well as theoretical nuclear researchers to study complete fusion and incomplete fusion (ICF) reaction dynamics [1-7]. Incomplete fusion (ICF) is used as a valuable tool in comprehensive reaction dynamics, and it is associated with the phase of nuclear interaction, thus acting as a crucial intermediary in shedding light on the transition from one body mean field at lower energy to two body nucleon-nucleon interactions at higher energies [5]. Experimental studies show that the ICF process predominantly occurs at energy above the coulomb barrier (V_{CB}) [2, 5]. Experimentally, Britt and Quinton first observed ICF reaction [6] following projectiles ^{12}C, ^{16}O, and ^{14}N break-up into alpha-cluster in an interaction with the target nuclei. Moreover, [7] provided remarkable information on ICF dynamics by the measurement employing the charged particle gamma coincidence technique.

Incomplete fusion depends on various parameters such as the coulomb effect [1, 8], deformation parameter, entrance channel mass asymmetry [9], projectile energy, etc. In the past, several dynamical models have been proposed to explain the mechanism of ICF reactions. The break-up fusion model of Udagawa and Tamura [10] based on Distorted Wave Born Approximation formalism explained ICF in terms of the break-up of the projectile in the vicinity of the target nuclear field. Wilczynski et al. [11] SUMRULE model proposed that the various ICF channels are localized in the angular momentum (ℓ)-space above the critical limit of angular momentum (ℓ_{crit}) for the CF to occur. CF reactions occur where the angular momentum imparted to the system is less or equal to ℓ_{crit} [12]. In a sharp cutoff approximation, the probability of CF is assumed to be unity for ℓ less or equal to ℓ_{crit} and expected to be zero for $\ell > \ell_{crit}$ [13], whereas at relatively higher projectile energies and finite values of the impact parameters, CF gradually gives way to ICF. Further dynamical models, like the exciton model [14], the hot spot model [15], the promptly emitted particles model [16], and the multistep direct reaction model [17], have been proposed to explain ICF dynamics. These entire models have been able to explain ICF dynamics at energy above 10MeV/nucleon. Various research groups have previously investigated incomplete fusion reaction properties using different projectile-target systems and energy ranges.

Pushpendra et al. [12] studied the underlying aspects of incomplete fusion by the spin distribution of the ^{16}O + ^{169}Tm system at ≈5.6 MeV/nucleon. The study found that the measured normalized production yields of fusion-evaporation xn/αxn-channels generally agree with the PACE4 predictions. Further, the results showed that products from the complete fusion reactions are strongly fed over a broad spin range, while evaporation residues from the incomplete fusion process are found to be less populated in the lower spin states, which are strongly hindered.

F. K. Amanuel et al. [2] Investigated the influence of incomplete fusion on the complete fusion of ^{12}C-induced reactions at ≈ 4–7.2 MeV/nucleon. It was found that for α-emitting channels populated in the interaction of ^{12}C+^{93}Nb, ^{12}C+^{59}Co, and ^{12}C+^{52}Cr projectile-target systems, the experimentally measured excitation functions were higher than the prediction of the theoretical model. Furthermore, it was found that the estimated incomplete fusion fraction, which represents the relative contribution of ICF to the total fusion reactions, is sensitive to the projectile energy and mass asymmetry of the entrance channel.

Ali et al. [18] studied the dynamics of incomplete fusion in ^{20}Ne+ ^{159}Tb systems; the study showed that the presence of significant ICF, resulting from the break-up of ^{20}Ne into ^{16}O + ^{4}He, ^{12}C+ ^{8}Be and ^{8}Be + ^{12}C, involves partial momentum transfer, leading to small recoil ranges where one of the fragments undergoes fusion with the ^{159}Tb target nucleus. Moreover, it was found that the estimated incomplete fusion fraction, which represents the relative contribution of ICF, is influenced by the function of various entrance channel parameters, such as mass asymmetry, coulomb factors, deformation parameters, and zeta parameters.

Kaur et al. [19] recently studied the reaction dynamics involved in the interaction of ^{12}C-projectile with ^{181}Ta-target near the coulomb barrier. Results showed that for non α-emitting channels populated in the interaction of the ^{12}C + ^{181}Ta system, the theoretical predictions using PACE4 agreed with the experimentally measured cross-section values. However, for α-emitting channels, enhancements on the experimentally measured cross sections over the PACE4 predictions were observed. It was confirmed that the observed enhancement for the α-emitting channel is attributed to the contribution of ICF reactions. Further in the study, a 7.7% contribution to the ICF reaction was found.

Much work has been done on studying ICF reactions for various target nuclei over a wide range of energy. However, reasonable comparative studies on ICF have been confined to beam energies greater than 10 MeV/nucleon. Furthermore, precise and robust modeling of ICF processes is still lacking, especially at relatively low bombarding energies ≈ 3-9 MeV/nucleon and for a few projectile-target systems. The present study seeks to contribute to addressing the gaps identified above; we study the effects of projectile energy and entrance channel mass-asymmetry on ICF reaction of ^{12}C + ^{128}Te, ^{12}C + ^{141}Pr, ^{12}C + ^{159}Tb, ^{16}O + ^{130}Te, ^{16}O + ^{159}Tb and ^{16}O+^{181}Ta projectiles + targets systems at ≈ 3-9 MeV/nucleon. For theoretical prediction, PACE4 code with 100,000 decay events was used. Furthermore, the Morgenstern [20] systematic was used to separate the ICF reaction cross-section contribution.

1.1.Objective

1.1.1. General objective

- To study the association between incomplete fusion and projectile energy and entrance channel mass-asymmetry in some ^{12}C/^{16}O-induced reactions

1.1.2. Specific objective

- To select values of sensitive input parameters that reproduced the measured data for representative non-α emitting channels.
- To deduce the contribution of incomplete fusion cross-sections
- To calculate the contribution of incomplete fusion fraction

CHAPTER TWO

2. THEORETICAL BACKDROUND OF NUCLEAR REACTION

2.1.Nuclear reaction

Nuclear reaction is described by identifying the incident particle, target nucleus and reaction products. It formed when two nuclei, or a nucleon and a nucleus, come together in such close contact that they interact through the strong force. Thus the energy must be high enough to overcome the natural electromagnetic repulsion between protons. If energy below the barrier, the nuclei will bounce off each other. Consider reaction represented by:

$$^{2}_{1}H + {}^{A}_{Z}X \rightarrow {}^{A}_{Z}X^{*} + p \ldots\ldots\ldots\ldots\ldots\ldots\ldots\ldots (2.1).$$

In which only the proton emerges. Here ${}^{A}{}_{Z}X$ is the target nucleus and ${}^{A}{}_{Z}X^{*}$ is its isotope (perhaps unstable) with one more neutron. The * denotes a possible excited state [21]. A low energy alpha particle from naturally radioactive materials is to bounce off target atoms and measure the size of the target nuclei (Rutherford Experiment's).

In nuclear reaction particle can collide and share energy using electromagnetic waves. However the rule must be followed during value of energy, mass and charge are not lost. So, whenever their exchange of energy, mass, or charge comes into play to make sure everything stays in balance. Conservation law in nuclear reaction are a set of laws and relationships that establish how quantity are conserved in nuclear interaction; the law of conservation of mass and energy, the law of momentum conservation, the Baryon number conservation, the lepton number conservation and the charge conservation [22]. However, quantities like magnetic dipole moments and electric quadrupole moments of the reacting nuclei which depend upon the internal distribution of mass, charge and current within the nuclei are not conserved [23].

Total relativistic energy conservation in basic reaction given by [24]:

$$m_x c^2 + T_x + m_a c^2 + T_a = m_y c^2 + T_y + m_b c^2 + T_b \quad \text{--------} \ (2.2).$$

Where, T, kinetic energy, in low energy relativistic approximation $T=1/2mv^2$, m's, are rest masses. C is speed of light.

The reaction Q value, in analogy with radioactive decay Q values, defined as the initial mass energy minus the final mass energy:

$$Q = (m_{initial} - m_{final})c^2 = (m_x + m_a - m_y - m_b)c^2 \quad \text{---------} \ (2.3).$$

It is the same as the excess kinetic energy of the final products:

$$Q = T_{final} – T_{initial} = T_b + T_y – T_a – T_x \text{ ---------- (2.4).}$$

The condition of Q value can be positive, negative or zero. Positive Q value ($m_{initial}$ > m_{final}or T_{final} >$T_{initial}$) the reaction is exoergic or exothermic, and nuclear mass or binding energy released as kinetic energy of the final products. Negative Q value ($m_{initial}$ < m_{final} or T_{final} <$T_{initial}$) the reaction is endoergic or endothermic, and initial kinetic energy is converted into nuclear mass or binding kinetic energy. The change in mass and energy can be related by expiration from special relativity, E=mc^2 any change in kinetic energy of the system of reacting particles must be balanced by an equal change in its rest energy ref[24].

2.2.Nuclear Reaction Mechanisms

Nuclear reaction mechanisms are classified into three based on interaction time, interacting particles and their relative energy. These are direct reaction, compound nucleus reaction and pre-equilibrium reaction. Those processes combine to give the inelastic cross-sections and all the other non-elastic reactions.

2.2.1. Direct Reaction

Direct reaction occurs when reaction passes from the initial to final state in a single state [28] in the time the projectile takes to traverse the target nucleus (~10^{-22} s). In this reaction, the projectile may interact with a nucleon; a group of nucleons or with the whole nucleus and emission takes place immediately. We write a reaction thus:

$$A + c \rightarrow B + d + Q \quad or \quad A(c,d)B ----------- (2.5).$$

A is the target, c is the projectile, B the residual, d is the ejectile and Q is the “Q value”. Each possible combination of particles is referred to as a partition. Further, within a partition we may specify the state of excitation of each nucleus. Such a pair of nuclei each in a specific state is known as a channel. Each partition can in principle consist of many channels. Thus the combination A + c are known as the entrance channel (both nuclei are in their ground states). The various possible sets of products B and d in their specific excitation states constitute the exit channels**.**

Some classes of direct reactions are;

(1) Elastic scattering. In elastic scattering the internal states of projectile (c) and target (A) in equation (2.5) are unchanged and Q =0. It is also written as: A (a, a) A.

(2) Inelastic scattering. Usually, this term is applied to a reaction where A is left in an excited state, i.e. B = A* and therefore $Q = -E_x$, **a,** is then emitted with reduced energy and the reaction is written as: A (a, a′) A*. For complex projectiles **a** may be excited instead of the target or both c and A may be left in excited states (mutual excitation).

(3) Transfer reactions. Here B ≠ A and c ≠ d, there has been a rearrangement (transfer) of nucleons between target and projectile. Two sub-groups conventionally defined in terms of the projectile:

Stripping ─ a nucleon or nucleons is transferred from the projectile to the target.

Pickup ─ a nucleon or nucleons is transferred from the target to the projectile.

(4) Breakup. This is no longer a simple two-body process but (usually) a three-body one: $A\,(a, a* \rightarrow b\, +\, c)A$ i.e. a, is excited to a "state" (either a resonance or the continuum) above the emission threshold for particle c (a, is considered to consist of particle c bound to core b) ref [28].

Direct reactions are widely used as a tool to study nuclear interactions and nuclear reaction dynamics. A proper quantum mechanical treatment has been developed for single-step reactions. Comparison between measured and calculated observables such as total and differential cross sections as well as angular distributions of the products is used to deduce information about the properties of the reactions and interacting nuclei. The nuclear structure of nuclei in the entrance and exit channel has a direct impact on direct reaction dynamics.

2.2.2. Compound nucleus reaction

Several nuclear reactions take place by the capture of a projectile to form a compound nucleus in an excited energy state which consequently decays by particle emission. In the time between its formation and decay all memory of its mode of formation is lost, since the excitation energy is shared statistically among its constituent nucleons [27]. The formation and decay process are thus independent of each other. Nuclear reactions with not very high kinetic energy of colliding particles, at least up to 10 MeV, proceed in two stages through the mechanism of a compound nucleus.

The first stage of the reaction is the absorption of the bombarding particle by the target-nucleus and the production of an intermediate, or compound, nucleus. The compound nucleus is always highly excited because the absorbed particle brings both its kinetic energy and the bond energy of the absorbed nucleons into the produced nucleus. The last component of the excitation energy is equal to the bond energy difference of the new nucleons in the compound nucleus and in the original particle if this particle is compound, as, for example, α particle.

The second stage of the reaction is the decay of the compound nucleus with the emission of this particle. The original particle may always be such a particle, and here again the original nucleus is formed, and scattering is observed instead of nuclear reaction. Scattering with the production of a compound nucleus is called resonance scattering in distinction from potential scattering without production of a compound nucleus. Possible ways of the decay of the compound nucleus are called channels of nuclear reaction. For example compound nucleus given [29] below;

$$\alpha + N^{14} \rightarrow F^{18*} \rightarrow O^{17} + p ------------ (2.6).$$

The index (*) meaning that the compound nucleus has some energy excess. Due to many complicated nucleon motions takes place the nucleus F^{18*} has lost memory of the entrance channels.

Compound nucleus reactions are more important at low energies, and remain a fruitful source of information about nuclear structure. In recent years, however, it has been found that there is not such a sharp division between compound nucleus and direct reactions; it is possible for particles to be emitted after the first direct interaction but long before the attainment of statistical equilibrium characteristic of compound nucleus reactions.

2.2.3. Pre-Equilibrium Reaction

When hot liquid drop cools off by emitting one or more particle, the pre-equilibrium reaction (pre-compound reaction) to occur after the first stage of direct reaction is over but in relatively few collisions the compound nucleus evaporates long before the thermal equilibrium is reached. Their time scale is intermediate between the very fast direct reactions and the relatively slow compound nucleus reactions. Direct evidence for pre-equilibrium reactions is provided by the energy spectra of particles at relatively high energy particles. They show conspicuous deviation from the Maxwell distribution expected from compound nucleus reactions and by the presence of peak from the excitation of low lying energy level due to direct reactions ref [23].

2.3. Heavy-ion reaction

This reaction refers to a nuclear reaction involving the collision of two heavy nuclei, typically heavier than protons and neutrons. Its interest with its roots in the quest to extend the periodic table beyond the elements that can be synthesized using neutrons and light charged particles and heavy actinide targets. Heavier beams of carbon, oxygen, and beyond were needed to reach this new boundary via the heavy ion fusion process in which the beam and target nuclei provided the protons and neutrons to the new element [30]. These reactions often occur at high energies and can lead to the formation of compound nuclei, particle emissions, and various nuclear processes.

B. B. Back et.al.[30] describes heavy-ion fusion reactions in terms of coupled-channels calculations. The major goal of these calculations is to provide a consistent description of all reaction channels including fusion, elastic and inelastic scattering, and transfer reactions.

Fusion reactions involve the merging of two heavy nuclei to form a single, heavy nucleus. This process requires overcoming the coulomb repulsion between the positively charged nuclei, and typically occurs at high temperatures and energies. This reaction is classified in to complete and incomplete fusion reactions.

In elastic scattering, the colliding heavy ion interacts and exchange energy and momentum, but without any nuclear reactions occurring. The nuclei retain their initial identities and trajectories.

In inelastic scattering, the colliding heavy ions undergo a nuclear excitation or de-excitation process. This results in the emission of photons or the transfer of energy and angular momentum between the nuclei, altering their internal structure.

2.3.1. Complete Fusion Reaction

It formed when projectile completely fuses with the target nucleus, forming a highly excited compound system which may further decay via emitting the light nuclear particles and/or γ-rays subsequently during its de-excitation at equilibrium stage. In this fusion full equilibrium before decay is not required so it might differ from compound nucleus formation. It is the summation of direct complete fusion and indirect complete fusion (J. Rangel et al.) [31]. CF occurs where the angular momentum imparted to the system is $\leq \ell_{cr}$ [32]. In sharp cut-off approximation the probability of CF is assumed to be unity until $\ell \approx \ell_{cr}$ and expected to be zero for $\ell > \ell_{cr}$; while at relatively higher projectile energies and at finite values of impact parameters, CF gradually gives way to ICF.

2.3.2. Incomplete Fusion Reaction

ICF reaction refers to a type of nuclear reaction in which the projectile nucleus collides with the target nucleus, but only a fraction of the projectile nucleus fuses with the target nucleus. During an ICF reaction, some nucleons from the projectile nucleus are transferred to the target nucleus, leading to the formation of a compound nucleus, however the remaining part of the projectile nucleus retain its identity and continuous to move forward without fully merging with the target nucleus. Experimentally separate ICF from CF is unambiguously challenged (Avinash Agarwal et al.) [33] So combination of theoretical with experiment is may be separate the ICF component from CF events.

ICF can occur due to several factors of entrance channel parameters [33], including the energy and momentum of the colliding nuclei, the nuclear structure and colliding nuclei, and the specific interaction between the projectile and target nuclei. This phenomenon is interest in nuclear physics, as it provides insight in to the dynamics of nuclear reactions, the transfer of nucleons between nuclei, and the factors that influence the fusion reaction.

2.3.2.1. Incomplete fusion reaction models

To understand the reaction dynamics of ICF process various dynamical model have been developed and tested. Those theoretical models have been used to fit experimental data of ICF at projectile energy above 10 MeV/nucleon. Those models are; SUMRULE model, Break-up fusion model, promptly emitted model, hot spot model, fermi jet model, multistep direct reaction model, exciton model, overlap model and etc.

2.3.2.1.1. Promptly emitted particle model

PEP model ref [16] refers to a theoretical framework describing the timely release of particle in a given systems. It is also called fermi jet models (Bondorf et al. 1979) [36], it impression is that nucleons with sufficiently high momentum in either nucleus might just jet through the single-particle well of the other nucleus [37]. In this model is assumed that some of the interacting nucleons fail to fully equilibrate during the collision, leading to the emission of particles promptly after the initial interaction.

At whatever, a mutual interface area is established between the interacting nuclei, nucleons can be transferred from one nucleus to the other. The nucleons that are transferred from the donor to the recipient have their intrinsic Fermi velocities in the donor system and therefore these nucleons would have a different velocity in the recipient system, the change coming from the relative velocity (v_{rel}). In the recipient system, therefore, the transferred nucleons treated as classical point particles would move with a velocity

$$v_b = v_{rel} + v_a \text{ …………… (2.7).}$$

Where, v_a is the intrinsic velocity of the transferred nucleons in the donor system (the subscripts a, and b refer to the donor nuclei recipient nuclei respectively). The transfer of nucleons from one nucleus to the other is governed by the evolving barrier geometry. The kinetic energy of these particles in the recipient system is then given by:

$$E_b = \frac{1}{2}mv_b^2, = E_a + E_{rel} + 2\text{Cos}\alpha\sqrt{E_a}E_{rel} \text{ ……………………… (2.8).}$$

Where m is the nucleon mass, $E_a = \frac{1}{2}mv_a^2$, $E_{rel} = \frac{1}{2}mv_{rel}^2$ and α-is the angle between the intrinsic velocity v_a and relative velocity(v_{rel}). The `extra' energy gained by the transferred particle is compensated by the recoil loss suffered by the donor system. This is because the remnant donor system with A-1 nucleons travels after the transfer with a reduced relative velocity which is a consequence of the momentum conservation.

$$v_{rel}^{after} = v_{rel}^{before} - {v_a}/{(A-1)} \text{ …………………………………… (2.9).}$$

Where, v_{rel}^{after} is reduced relative velocity, v_{rel}^{before} is the relative velocity of the A-nucleon system just before the emission. The probability of PEP emission for a certain impact parameter is given by:

$$P_{PEP} = \int dt \int dA \int dv_a P(v_a) n(v_b) e^{-d/\lambda} \text{ …………………………………….. (2.10).}$$

Where, A refers to the mutual interface area, $n(v_b)$ is the local one-sided flux of nucleons passing through the mutual interface, d is the distance traversed by the prospective PEP inside the recipient and $e^{-d/\lambda}$ is the absorption factor, λ being the mean free path. The total PEP emission cross section is then given by:

$$\sigma_t = 2\pi \int_0^{b_g} bdbP_{PEP} \text{ …………………………… (2.11).}$$

Where, b_g is the grazing impact parameter, One can, however, divide the total cross section in two components, one coming from the compound reaction and the other coming from deep inelastic (and quasi elastic components) as:

$$\sigma_t = \sigma_{CF} + \sigma_{DI} \text{ ……………………………… (2.12).}$$

Frequently for deep inelastic processes there is only a small contribution to the total PEP emission cross section. Though the deep inelastic events involve peripheral or nearly peripheral collisions and therefore have a large geometrical factor. Those equation (2.7 – 2.12) pertains to the PEPs resulting from nucleons transferred from donor nuclei to recipient nuclei.

Obviously, those PEPs resulting from transfer from recipient nuclei to donor nuclei can be treated as similar manner and in fact all the formula hold also for those if the subscripts a and b are interchanged.

Factor that affect the PEP model of incomplete fusion dynamics are; projectile energy, target nucleus properties, angular momentum, excitation energy, spin orbit interaction and collective motion. Understanding and modeling these factors collectively contribute to a more comprehensive representation of the PEP model of incomplete fusion dynamics.

Limitation of PEP model of incomplete fusion dynamics are; simplified assumptions, empirical nature, incomplete consideration of reaction mechanisms, limited predictive power, nuclear structure effect, energy dependence, complexity of nuclear reaction and need of experimental validation. While the PEP model of incomplete fusion dynamics provides valuable insights, we should be aware of its limitations and use it sensibly, considering the specific conditions and nuclei for which it has been validated.

2.3.2.1.2. Break-up fusion model

This model considers the interaction between complete and incomplete fusion, providing insights into the dynamics of nuclear reactions. It defines ICF in terms of the break-up of the projectile in the nuclear force field of the target nucleus followed by fusion of one of the fragments with the target (Udagawa and Tamura et.al) ref [10]. It uses complex theoretical frameworks and numerical simulation rather than a single formula. Distorted Wave Born Approximation (DWBA) is a widely used theoretical approach that considers the breakup of the incident projectile into different channels during the collision. BUF model involve solving complex sets of differential equations, considering the interaction potentials and incorporating the effect of nuclear structure, angular momentum and other relevant parameters.

BUF model of incomplete fusion dynamics depends on many factors; projectile energy, angular momentum, nuclear structure, reaction mechanism, impact parameter, nuclear shell effect, cross section and mass asymmetry. Those factors collectively contribute to the complexity of incomplete fusion dynamics and the breakup fusion model aims to account for their interplay to describe the outcomes of nuclear reactions involving incomplete fusion.

The limitation of BUF model for incomplete fusion dynamics are; sensitivity to the model parameters, assumption about reaction mechanism, complexity of nuclear reactions, limited data for validation, influence of angular momentum, mass asymmetry effects, quantum tunneling and resonances. Despite these limitations, breakup fusion models provide valuable insights and are essential for understanding incomplete fusion dynamics. Researchers continually work to refine these models and address their limitations through improved theoretical approaches and experimental data collection.

2.3.2.1.3. SUMRULE model

The original sum rule model (OSRM) was proposed by Wilczyński et al. ref [11] to combine CF and ICF into a single framework. The model has been successfully utilized in explaining the experimentally observed cross section in the beam energy of around 10 MeV/nucleon. This model enabled us to calculate absolute cross section of i_{th} reaction channel, which is given as:

$$\sigma\,(\mathrm{i}) = \pi ƛ^2 \sum_{\ell=0}^{\ell max} (2\ell + 1)\, N_l T_l(\mathrm{i}) \mathrm{P}(\mathrm{i}) - - - - - - - - - - \quad (2.13).$$

Where ƛ is the reduced de Broglie wavelength, ℓ_{max} is the maximum angular momentum.

The reaction probability $P(i)$, for the i_{th} reaction channel (including CF), is proportional to the ground state Q-value ($[Q\mathrm{gg(i)} - Qc(i)]/_{T}$) where T is a parameter, $Q_c(i)$ is change in the Coulomb interaction energy and Q_{gg}(i) is ground state Q-value. Due to the transfer of charge $Q_c(i)$ is given by:

$$Q_c(i) = q_c\left(Z_1^f Z_2^f - Z_2^{in} Z_1^{in}\right)c^2 \;\ldots\ldots\ldots\ldots\ldots..(2.14).$$

Where Z_1^{in}, Z_2^{in} and Z_1^f, Z_2^f are the atomic numbers of the constituents of the di nuclear system before and after the transfer of charge, and q_c is a parameter. Each of the CF and ICF processes are viewed as forming di nuclear systems. This di nuclear system consists of the projectile and the target before the reaction takes place. After the fusion, the di nuclear system becomes an ejectile and the compound nucleus (target + captured fragment).

The limiting angular momentum $l_{lim}\ (i)$ is defined as [34]:

$l_{lim}\ (i)$ = (mass of projectile/mass of captured fragment) ℓ_{cr} (target + captured fragment).

The main feature of original sum rule model is the generalized concept of angular momentum. The quantity critical angular momentum (ℓ_{cr}) is an important ingredient and is calculated by the balance of nuclear and Coulomb forces when the target and captured fragment are at the sum of their half-density radii. The weakness of this model is does not involve the energy dependence of the projectile. To fill this gap the modified sum rule model was proposed [35].

2.3.2.1.4. Multi-step direct reaction model

Multi-step direct (MSD) reaction model ref [17] is a theoretical framework used to describe certain nuclear reactions, it consider the reaction occurring in multiple steps, involving intermediate states of the nuclear system. It helps to provide a more detailed and nuanced understanding of nuclear reactions, especially in cases where the direct interaction involves multiple steps. It has been applied to study incomplete fusion reactions, where the incident particle does not fully merge with the target nucleus but leaves it in an excited state.

Factor affecting the MSD reaction model are; incident particle characteristics, target nucleus properties, angular momentum transfer, excitation energy, deformation effect, spin orbit interaction, projectile structure, nuclear shell effect, and emission channel and energy conservation. Understanding and modeling these factors collectively contribute to a more comprehensive representation of the multi-step direct reaction model in incomplete fusion dynamics.

Limitation of multistep direct (MSD) reaction model are; complexity and computational demands, assumption and approximations, limited predictive power, sensitivity to model parametrizes, experimental challenge, influence of couplings, energy dependent limitation and incomplete description of nuclear structure. When we use this model we should be mindful of these limitations and use the model judiciously, considering its strengths and weakness in specific nuclear reaction.

2.3.2.1.5. Overlap Model

This model [38] depends on nuclear forces acting, because of their short range, mostly on that part of a nucleus which overlaps between target nucleus and the nucleons removed from the projectile. The forces can be considered either macroscopically, particularly as friction forces, or microscopically as the interaction between nucleons causing target-nucleon projectile-nucleon collisions. The effects of both forces increase with energy, macroscopic force being proportional to the velocity, microscopic decreasing with energy in favor of few particle capture, and that an ejectile is produced by collisions whose impact parameter decreases indefinitely as the projectile velocity increases. Obviously the high energy range is the proper domain for geometric models such as the abrasion mechanism, for detailed formula and calculation ref [38].

Some similarity and deference between overlap and SUMRULE model ref [37] are; both models confronting with data, they give similar predictions at some moderate bombarding energies up to 20 MeV, however at 35 MeV the models differ, and the experiment clearly favor's the overlap model. Both models also imply definite and easily calculable angular-momentum transfers. Their difference on the excitation functions, the excitation function of overlap model reproduce the measured cross sections of fast forward-emitted fragments rise steeply and then level off approaching the geometric limit. The onset energies rise with increasing mass loss, from few-nucleon stripping to the massive transfer (Ne, α). However contradict the sum-rule model with its inverted ordering of onset energies-from fusion over incomplete fusion, (Ne, α), to less and less complete fusion and the fall-off of cross sections at higher energies.

2.3.2.1.6. Exciton model

This model ref [14] is a theoretical framework that is used to explain incomplete fusion reaction based on the concept of exciton, which are quasi particle that represent the collective behavior of excited number states. In this model the interacting nuclear system is treated as a collection of excitons, where each exciton corresponding to a specific exciton mode of the system. The incomplete fusion reaction is then described as the transfer of one or more excitons from the projectile to the target nucleus.

This model assumes that the nuclear system can be divided into two parts; the core and the valence nucleons. The core is the tightly bound nucleons in the nucleus while the valence nucleons are more loosely bound and can be transferred between the colliding nuclei. During an incomplete fusion reaction, the valence nucleons are transferred from the projectile to the target nucleus, forming an excited compound nucleus.

2.3.2.1.7. Hotspot model

This model ref [15] is a theoretical framework that based on the concept of the formation of a localized in the colliding nuclei during the reaction. The colliding nuclei form a compound nucleus for a brief moment, this compound nucleus is characterized by localized region of increased density and excitation energy, referred to as the hotspot, this hotspot is formed due to the strong interaction between nucleons and their clustering with the nucleus.

In this model, incomplete fusion reactions occur when the incoming projectile nucleus collides with the target nucleus to form the compound nucleus, while the remaining part of the projectile nucleus passes away. The incomplete fusion process is influenced by factor such as the projectile energy, the collision impact parameter and property of the colliding nuclei.

When it comes to explaining ICF reaction this model have some limitations those are; simplified assumptions, lack of microscopic details, neglect nuclear structure effects and limited applicability.

2.4. Nuclear Reaction Cross Sections

Cross sections are the probability that a certain reaction will occur between two particles for a given set of parameters. Basically, a cross section can be roughly thought of as a target, like one at a bombardment range. The probability that a reaction will occur is analogous to the probability of a random bullet hitting its target. The reaction cross-section can be visualized as an effective area around the nucleus such that if the incident particles cross that area, a nuclear reaction takes place, otherwise not. This area is also known as effective area. It is not exactly same as the geometrical area($pr2$), where r is the radius of the nucleus. This effective area could be larger, smaller or equal to the geometrical area of the nucleus. Thus, nuclear cross-section is a measure of the probability that bombarding particles at a particular energy would interact with the target [25]. There are two kinds of cross sections, microscopic and macroscopic. Microscopic cross section refers to cross sections of neutrons reacting with a specific atom, like the isotope U^{235}. While macroscopic cross section gives a description how neutrons interact with bulk materials such as concrete, water, steel, etc. Both cross section are determined experimentally by;

$$\Delta P = \frac{\rho N_A}{M} \sigma \Delta d \text{ --------- } (2.15).$$

Where, ΔP being the change in probability that a reaction occurs for a given change in penetration distance Δd, N_A is Avogadro's number, M is the atomic (molecular) mass, ρ is the density, and σ is the cross section of being measured. Cross sections have units of area and are given in units of m^2 or barns (where 1 barn = 10^{-28} m^2) [26]. Detail of compound nucleus reaction cross section is stated in section 3.2 of this thesis.

2.4.1. Partial Wave Analysis

Method of partial wave analysis can be used to solve 3D scattering problems with spherically symmetric scattering potentials. Such a potential, V (r), depends only on the radial distance r $=\sqrt{x^2 + y^2 + z^2}$ and not on direction. This typically describes a situation where a point particle or spherically-symmetric object sits at the coordinate origin, r = 0, and is bombarded by incident particles. At distances of separation larger than the range R of the potential the projectile can be described by a plane wave moving along the z-axis, which is then scattered in the spherically symmetrical potential V (r).

Let us consider Schrödinger equation given by:

$$\frac{-\hbar^2}{2\mu}\overrightarrow{\nabla^2}\,\psi(\overrightarrow{r})+\hat{V}(r)\psi(\widehat{r})= \mathrm{E}\,\psi(\overrightarrow{r}) \text{ ……………… (2.16).}$$

The general solution of equation 2.16 is given by:

$$\psi(\overrightarrow{r}) = \sum_{lm} C_{lm} R_{kl}(r) Y_{lm}(\theta,\ \varphi) \text{ …………………………. (2.17).}$$

Where, $R_{kl}(r)$is radial part of wave function and $Y_{lm}(\theta, \varphi)$is angle part of wave function. Since V(r) is central; the system is symmetrical about the Z-axis. The scattered wave function must not depend on the azimuthal angleφ: i.e. m=0 thus, angle part of wave function becomes$\approx P_l cos\theta$, so the equation (2.17) becomes:

$$\psi(r,\theta)=\sum_{l=0}^{\infty} a_l R_{kl}(r) P_l(cos\theta) \text{ ……………………. (2.18).}$$

Where, $R_{kl}(r)$obeys the following radial equation:

$$\left[\frac{d^2}{dr^2}+\ k^2-\ \frac{l(l+1)}{r^2}\right](rR_{kl}(r))=\frac{2m}{\hbar^2}V(r)(rR_{kl}(r)) \text{ ……………….. (2.19).}$$

At large value of r, the scattering potential is effectively zero. Then equation (2.19) becomes:

$$\left(\frac{d}{dr^2}+\ k^2\right)(rR_{kl}(r)=0 \ldots\ldots\ldots\ldots\ldots\ldots\ldots\ldots\ldots\ldots\ldots\ldots (2.20).$$

General solution of equation (2.20) is given by linear combination of the spherical Bessel and Neumann functions:

$$R_{kl}(r)= A_l J_i(kr)+\ B_l n_l(kr) \ldots\ldots\ldots\ldots\ldots\ldots\ldots\ldots\ldots\ldots\ldots\ldots\ldots\ldots\ldots (2.21).$$

Where, $J_i(kr)$ and $n_l(kr)$ are Bessel function and Neumann function respectively and their asymptotic form are given in equation (2.22) and (2.23).

$$J_l(kr)\rightarrow\frac{\sin(kr-{l\pi}/{2})}{kr} \ldots\ldots\ldots\ldots\ldots\ldots\ldots\ldots\ldots\ldots (2.22).$$

$$n_l(kr)\rightarrow-\frac{\cos(kr-{l\pi}/{2})}{kr} \ldots\ldots\ldots\ldots\ldots\ldots\ldots\ldots\ldots (2.23).$$

Let, we substitute equation (2.22) and (2.23) into (2.21), we get asymptotic form of radial equation.

$$R_{kl}(r)\rightarrow A_l\frac{\sin\left(kr-{l\pi}/{2}\right)}{kr}-B_l\frac{\cos(kr-{l\pi}/{2})}{kr}\ldots\ldots\ldots\ldots\ldots\ldots\ldots\ldots\ldots\ldots (2.24).$$

Since, r=0, the solution of radial equation (2.20) is vanish; thus $R_{kl}(r)$ must be finite at the origin. We introduce the phase shift δ_l to achieve the regular solution near the origin by rewriting equation (2.21):

$$R_{kl}(r)=C_l[\cos(\delta_l)\,j_l(kr)-\sin(\delta_l)n_l(kr)]\ldots\ldots\ldots\ldots\ldots\ldots\ldots\ldots (2.25).$$

We have $A_l=C_l cos\delta_l$ and $B_l=-C_l sin\delta_l$ $C_l=\sqrt{A_l^2+B_l^2}$ $\delta_l=tan^{-1}\left({B_l}/{A_l}\right)$.

Using equation (2.25) we can write asymptotic limit of the scattered wave function of equation (2.18) as:

$$\Psi(\mathrm{r},\theta)\rightarrow\sum_{l=0}^{\infty}a_l P_l(cos\theta)\frac{\sin(kr-{l\pi}/{2}+\delta_l)}{kr} \ldots\ldots\ldots\ldots\ldots\ldots\ldots\ldots (2.26).$$

This wave function (2.26) is known as a distorted plane wave, which differs from a plane wave by the phase shift δ_l. Since, $\sin\left(kr - {}^{l\pi}/_{2} + \delta_l\right) = {}^{\left[(-i)^l e^{ikr} e^{i\delta_l} - i^l e^{-ikr} e^{-i\delta_l}\right]}/_{2i}$ equation (2.26) can be rewrite as:

$$\psi(r,\theta) \to -\frac{e^{ikr}}{2ikr}\sum_{l=0}^{\infty} a_l i^l e^{-i\delta_l} P_l(cos\theta) + \frac{e^{ikr}}{2ikr}\sum_{l=0}^{\infty} a_l (-i)^l e^{i\delta_l} P_l(cos\theta) \text{ .... (2.27).}$$

We can also write scattering wave function as:

$$\psi(r,\theta) \approx \sum_{l=0}^{\infty} i^l (2l+1) j_l(kr) P_l(cos\theta) + f(\theta)\frac{e^{ikr}}{r} \text{ .... (2.28).}$$

By comparing equation (2.27) and (2.28) we get:

$$a_l = (2l+1) i^l e^{i\delta_l} \text{ .... (2.29).}$$

By substituting equation (2.29) into (2.27) we get:

$$\psi(r,\theta) \to -\frac{e^{ikr}}{2ikr}\sum_{l=0}^{\infty}(2l+1) i^{2l} P_l(cos\theta) + \frac{e^{ikr}}{2ikr}\sum_{l=0}^{\infty}(2l+1) i^l (-i)^l e^{2i\delta_l} P_l(cos\theta) \ldots \ (2.30).$$

Let, as equate equation (2.28) and (2.30) and multiply the whole by factor, $\frac{r}{e^{ikr}}$ we get:

$$f(\theta) = \sum_{l=0}^{\infty} f_l\,(\theta) = \frac{1}{k}\sum_{l=0}^{\infty}(2l+1) e^{i\delta_l} sin\delta_l P_l\,(cos\theta) \text{ .... (2.31).}$$

Where, $f_l(\theta)$ is partial wave amplitude, Know we can obtain the differential cross sections from equation (2.31):

$$\frac{d\sigma}{d\Omega} = |f(\theta)|^2 = \frac{1}{k^2}\sum_{l=1}^{\infty}\sum_{l'=1}^{\infty}(2l+1)(2l'+1) e^{i(\delta_l - \delta_{l'})}\ sinlsinl' P_l(cos\theta) P_{l'}(cos\theta) \ldots \text{ (2.32).}$$

Although, the total reaction cross sections can be given as:

$$\sigma = \int_0^{\pi} \frac{d\sigma}{d\Omega} d\Omega = \int_0^{\pi} |f(\theta)|^2 sin\theta d\theta \int_0^{2\pi} d\varphi = 2\pi \int_0^{\pi} |f(\theta)|^2 sin\theta d\theta$$

$$= \frac{2\pi}{k^2}\sum_{l=0}^{\infty}\sum_{l'=0}^{\infty}(2l+1)(2l'+1) e^{i(\delta_l - \delta_{l'})} sin\delta_l sin\delta_{l'} \int_0^{\pi} P_l P_{l'} sin\theta d\theta \ldots\ldots\ldots\text{(2.34).}$$

Let, as use the relation of $\int_0^{\pi} P_l(cos\theta)P_{l'}(cos\theta)sin\theta d\theta = \left[\frac{2}{(2l+1)}\right]\delta_{ll'}$, we can obtain the partial cross sections corresponding to the scattering of particles in various angular momentum states.

$$\sigma = \sum_{l=0}^{\infty} \sigma_l = \frac{4\pi}{k^2}\sum_{l=0}^{\infty}(2l+1)sin^2\delta_l \dots\dots\dots\dots\dots (2.35)$$

Equation (2.35) is represents partial cross section of scattering particles in various angular momentum states.

CHAPTER THREE

3. FORMULATION AND PACE4 CODE

Calculations based on theoretical nuclear reaction models play a very significant role in the development of reliable reaction cross-section data. In this work, excitation function calculations were performed using PACE4 reaction model codes. This chapter explains PACE4 and the Hauser-Feshbach formulation.

3.1. PACE4

The code PACE [39] is the fusion evaporation code of a modified version of JULIAN - the Hillman Eyal evaporation code. PACE4 (Projection Angular-momentum Coupled Evaporation version 4) uses a Monte-Carlo code coupling angular momentum to determine the decay sequence of an excited compound nucleus using the statistical Hauser-Feshback formula.

The advantage of this code is that it has a user-friendly interface in the MS Windows system, where the user can enter information directly in dialogs, in which the explanation for each parameter is displayed. The entered information is written in files with the extension "in" and is compatible with the previous versions. Its calculation provides correlations between various quantities, such as particles and γ rays or angular distribution of particles. It also provides the ability to have an event-by-event trace back of the entire decay sequence from the CN system into any one of the exit channels [40].

Theoretical data were generated by entering some variable input parameters (like exciton number, level density, etc.) and the energy ranges of the projectile obtained from experimental data of EXFOR into the software package known as computer code, PACE4. The selected computer code was run to find an optimized input parameter value that should cover the entire energy spectrum.

The equilibrium state components of the cross-section are primarily affected by level density parameter (**a**) ref [2], in this code (**a)** calculated from the expression **a** = A/K MeV−1, where A is the nucleon number of a compound system, and K is an adjustable constant, which may be varied to match the experimental data. The experimentally measured EFs were compared with PACE4 predictions for different level density parameter values for representative evaporation residues in some ^{12}C/ ^{16}O induced reaction systems produced only via the CF processes. In this work, by running this computer code, the value of K that matches with experimental data was selected.

3.2. Hauser-Fechbach Formulation

The formulation of Hauser-Fechbach theory gives the cross-section of reactions that pass through a large number of compound nucleus states [27]. The initial form of Hauser-Fechbach's theory is based on the Bohr independence hypothesis. Bohr hypothesis permits the cross-section to be written as the product of two factors: the cross-section σ_a for the formation of the compound nucleus and the probability P_β that it will decay into the channel β [47] and is given by:

$$\sigma_{\alpha\beta}=\sigma_\alpha P_\beta \quad \text{……………… (3.1)}$$

The compound nucleus formation cross section for a particular orbital angular momentum is given by:

$$\sigma_a=\pi\lambda\!\!\!^{-2} T_a \quad \text{……………………… (3.2)}$$

Where, ƛ reduced wavelength, T_a=1- $|S_a|^2$ is the transmission coefficient in the α-channel and S_a is elements of matrices.

For the CN formation, the partial cross-section σ_l related to the individual angular momentum (ℓ) values at particular incident energy is also given by:

$$\sigma_\ell = \pi\lambda^2(2\ell + 1)T_\ell \quad \text{……………………………………… (3.3)}$$

Where the transmission coefficient (T_ℓ) is taken to be:

$$T_\ell=[1+\exp(\frac{l-l_{max}}{\Delta}]^{-1} = \frac{T_\alpha}{2l+1} \text{……………………… (3.4)}$$

Let we use the reciprocity theorem that relates a cross-section to its inverse:

$$\lambda\!\!\!^{-}{}_\alpha^2\sigma_{\alpha\beta}=\lambda\!\!\!^{-}{}_\beta^2\sigma_{\hat{\alpha}\hat{\beta}} \quad \text{………………………... (3.5)}$$

Here, $\hat{\alpha}$ and $\hat{\beta}$ refer to time-reversed states. The combination of equations (3.1), (3.2), and (3.5) gives that:

$$T_\alpha P_\beta=T_{\hat{\beta}}P_{\hat{\alpha}} \quad \text{…………………….. (3.6)}$$

Meanwhile, this is true for all channels α andβ, so equation (3.6) can be written as:

$$\frac{P_{\hat{\alpha}}}{T_\alpha} = \frac{P_\beta}{T_{\hat{\beta}}} = \lambda \quad \text{…………………………….. (3.7)}$$

Where λ is constant, P is probability and so it can be written as:

$$\sum_\alpha P_{\hat{\alpha}} = \lambda\sum_\alpha T_\alpha = 1 \quad \text{……………………………. (3.8)}$$

From equations (3.7) and (3.8), we can also write the probability of outgoing channel β as:

$$P_\beta = \lambda T_{\widehat{\beta}} = \frac{T_{\widehat{\beta}}}{\sum_\alpha T_\alpha} \ldots\ldots\ldots\ldots\ldots\ldots\ldots\ldots\ldots\ldots\ldots\ldots (3.9)$$

Therefore, by combining equations (3.1), (3.2), and (3.9), we get:

$$\sigma_{\alpha\beta} = \pi\lambda_\alpha^2 \frac{T_\alpha T_{\widehat{\beta}}}{\sum_i T_i} \ldots\ldots\ldots\ldots\ldots\ldots\ldots\ldots\ldots (3.10)$$

Equation (3.10) is called Hauser-Feshbach formula in its simplest form. It gives the cross-section of a compound nucleus reaction from a single incident channel α to a single outgoing channelβ, for a particular angular momentum ℓ in the absence of spin. However, if the interacting particles have spin, the expiration for the cross section must include the appropriate spin weighting factors. The extended formula consists of the possibility that branching ratios vary with J; the spin of the compound nucleus [47] is given by:

$$\sigma_{ab} = \frac{\pi ƛ^2}{(2I_1+1)(2I_2+1)} \sum_{J,\pi} (2J+1) \frac{\sum_{\alpha,\beta} T_{a\alpha} T_{b\beta}}{\sum_{\gamma,c} T_{c\gamma}} \ldots\ldots\ldots\ldots\ldots\ldots\ldots\ldots (3.11)$$

Here, $\sigma_{ab}$is the cross section for the reaction$A(a,b)B$. Where, a, is bombarding particle, A-target particle, b-emitted particle, and B-residue. J is the compound nucleus's total angular momentum, and π denotes the parity. I_1- Spin of the target and I_2 - spin of the projectile. $T_{a\alpha}$ - Transmission coefficient for the entrance channel, α angular momentum in this channel, $T_{b\beta}$ - transmission coefficient in the exit channel, and β denotes the angular momentum in the exit channel. ƛ - Reduced wavelength of the incident particle.

In this work, after we calculated the excitation function using PACE4, ICF cross-section for individual α-emitting channels that points towards the presence of ICF process in the formation of all evaporation residues were calculated as:

$$\sigma_{ICF} = \sigma_{exp} - \sigma_{CF} \ldots\ldots\ldots\ldots\ldots\ldots\ldots\ldots (3.12)$$

The total ICF cross-section for a given system was determined using the relation:

$$\sigma_{ICF}(\text{Total}) = \sum \sigma_{ICF}(\text{individual}) \ldots\ldots\ldots\ldots\ldots\ldots\ldots\ldots (3.13)$$

To see the correlation between ICF andE_{lab} a comparison of σ_{ICF}(total) versus E_{lab} for each system and a comparison of σ_{ICF} (total) versus E_{lab}/V_{CB} and F_{ICF} (%) versus E_{lab}/V_{CB} for all systems under investigation were considered. E_{lab} obtained from EXFOR data, and the effect of Coulomb barriers (V_{CB}) were calculated as:

$$V_{CB} = \frac{Z_P Z_T}{A_P^{1/3} + A_T^{1/3}} \text{ ------------ } (3.14)$$

To see the correlation between ICF and entrance channel mass-asymmetry, the comparison of the percentage of incomplete fusion fraction (F_{ICF}) versus normalized relative velocity ($^{v_{rel}}/_{c}$) for all systems under investigation was considered. Where F_{ICF} and V_{rel} were calculated as:

$$F_{ICF} = \frac{\sum \sigma_{ICF}}{\sum \sigma_{Exp}} \quad \text{------------ (3.15)}$$

$$v_{rel} = \sqrt{\frac{2(E_{c.m} - V_{CB})}{\mu}} \quad \text{----------- (3.16)}$$

Where μ is the reduced mass of the system, were calculated as: $\mu = \frac{A_P\, A_T}{A_T + A_P}$ ---------- (3.17)

$E_{c.m.}$ is the center-of-mass energy, was calculated as: $E_{CM} = \frac{A_T}{A_T + A_P} E_{lab}$ ------------ (3.18)

CHAPTER FOUR

4. RESULT AND DISCUSSION

In this chapter, the contribution of incomplete fusion reactions from ^{12}C + ^{128}Te, ^{12}C + ^{141}Pr, ^{12}C + ^{159}Tb, ^{16}O + ^{130}Te, ^{16}O + ^{159}Tb and ^{16}O + ^{181}Ta projectiles + targets systems were induced up to 106 MeV. Excitation functions various residues populated in the interactions of ^{12}C + ^{128}Te, ^{12}C + ^{141}Pr, ^{12}C + ^{159}Tb, ^{16}O + ^{130}Te, ^{16}O + ^{159}Tb, and ^{16}O + ^{181}Ta projectiles + Targets systems were predicted theoretically using the statistical reaction model code PACE4, which doesn't take ICF contribution into account. We selected the PACE4 code in the theoretical prediction because, in the past, this code has been very successful in investigating reaction mechanisms for heavy ion-induced reactions [39]. In PACE4 code, the sensitive input parameter, the level density a, which primarily impacts the equilibrium state components of a reaction cross section, was calculated from the expression $a = A/K$ MeV^{-1}, where A is the number of nucleons in the composite nucleus (projectile + target), and K is an adjustable constant, which can be varied to match experimental data. In this work, a representative channel not populated by ICF from the respective systems was selected to select the best-fitted level density parameter value from the respective systems, and a comparison was made with the experimental data. The experimental cross-section data for possible residues populated in ^{12}C + ^{128}Te, ^{12}C + ^{141}Pr, ^{12}C + ^{159}Tb, ^{16}O + ^{130}Te, ^{16}O + ^{159}Tb, and ^{16}O + ^{181}Ta reactions are available in the EXFOR database [41-46].

To show the best-fitted level density value selection processes, we present a representative $^{159}Tb(^{12}C, 4n)^{167}Lu$ channel not populated by the ICF process from the ^{12}C + ^{159}Tb system. Figure 4.1 displays the experimentally measured and theoretically predicted (K=8, 10, 12 values) excitation function of ^{167}Lu populated in the interaction of ^{12}C with ^{159}Tb. As can be seen from Figure 4.1, the predicted excitation functions corresponding to the level density parameter K=10 in general reproduced satisfactorily experimentally measured one. We consistently followed the same approach for the remaining projectiles + target systems.

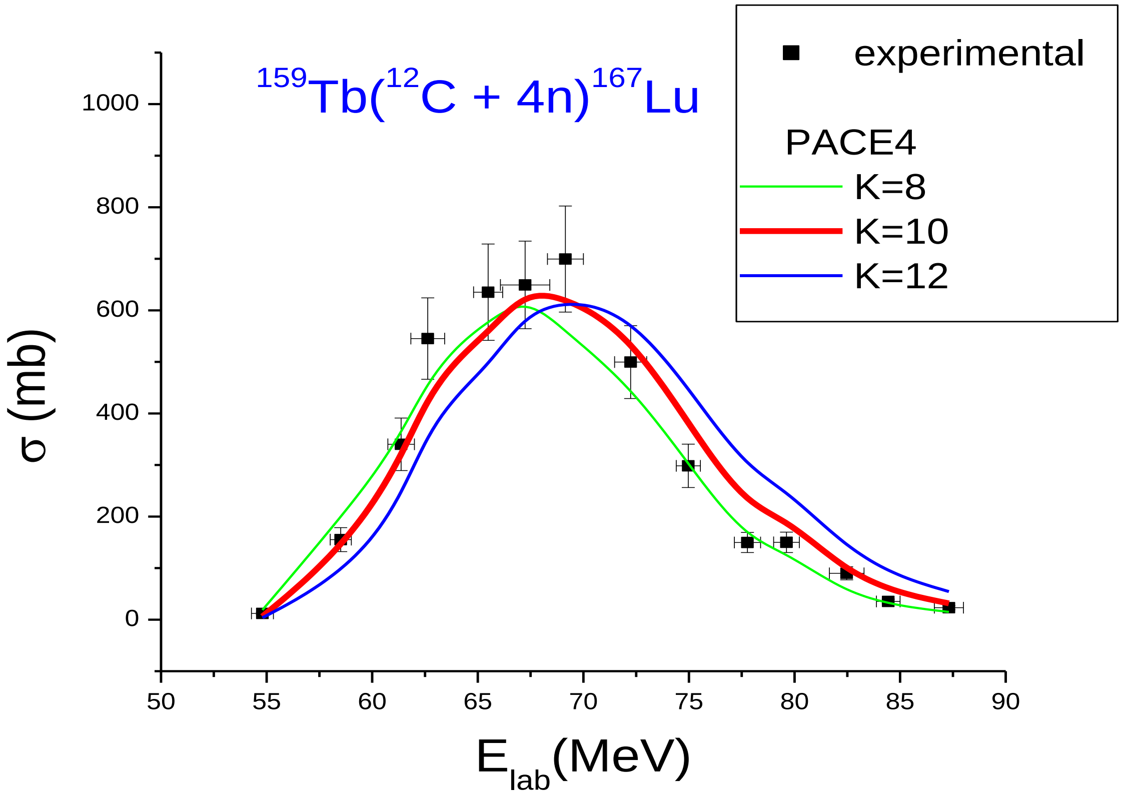

Figure 4.1: Experimentally measured and theoretically calculated EFs for residue ^{167}Lu populated via the CF channels of (^{12}C, 4n) in the ^{12}C + ^{159}Tb system within the energy range ≈ 55-87 MeV.

4.1. Deduction of incomplete fusion cross-sections

4.1.1. ^{12}C-induced reactions

a) ^{12}C + ^{128}Te system

In ^{12}C + ^{128}Te system ^{133}Ba, ^{131}Ba and ^{131}Te residues are populated through CF and ICF respectively via (^{12}C, α3n), (^{12}C, α5n) and (^{12}C, α4pn) channels. Figure 4.2 displays the theoretical excitation functions and the measured EFs for a representative (^{12}C, α3n) channel populated via CF and ICF reactions in ^{12}C + ^{128}Te. As seen from this figure, the experimentally measured EF is higher than the prediction of PACE4. The observed difference between the two cross sections is attributed to the contribution of ICF (σ_{ICF} (^{133}Ba) = $\sigma_{experimental} - \sigma_{PACE4}$ since the PACE4 code doesn't consider ICF reaction.

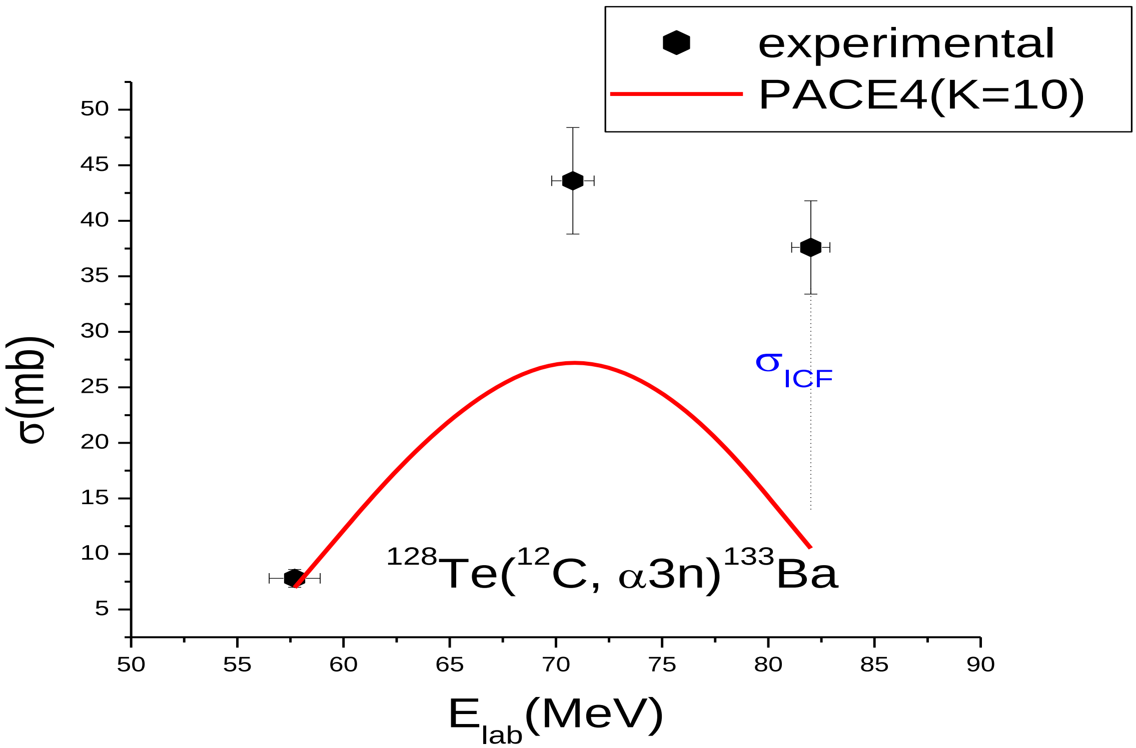

Figure 4.2: Theoretical excitation functions along with the measured EFs for a representative (^{12}C, α3n) channel populated via CF and ICF reactions in ^{12}C + ^{128}Te.

To find the contribution of the total ICF cross-section, $\Sigma\sigma_{ICF}$, in the ^{12}C + ^{128}Te system, we sum up individual residue ICF contribution, which is the difference between experimental cross-section and PACE4 prediction.

$\Sigma\sigma_{ICF}$= σ_{ICF}(^{133}Ba) + σ_{ICF}(^{131}Ba) + σ_{ICF}(^{131}Te)

Figure 4.3 shows the deduced total ICF cross-section, $\Sigma\sigma_{ICF}$, and projectile energy. As can be seen from this figure, the total incomplete fusion reaction cross-section in the ^{12}C + ^{128}Te system increases with projectile energy.

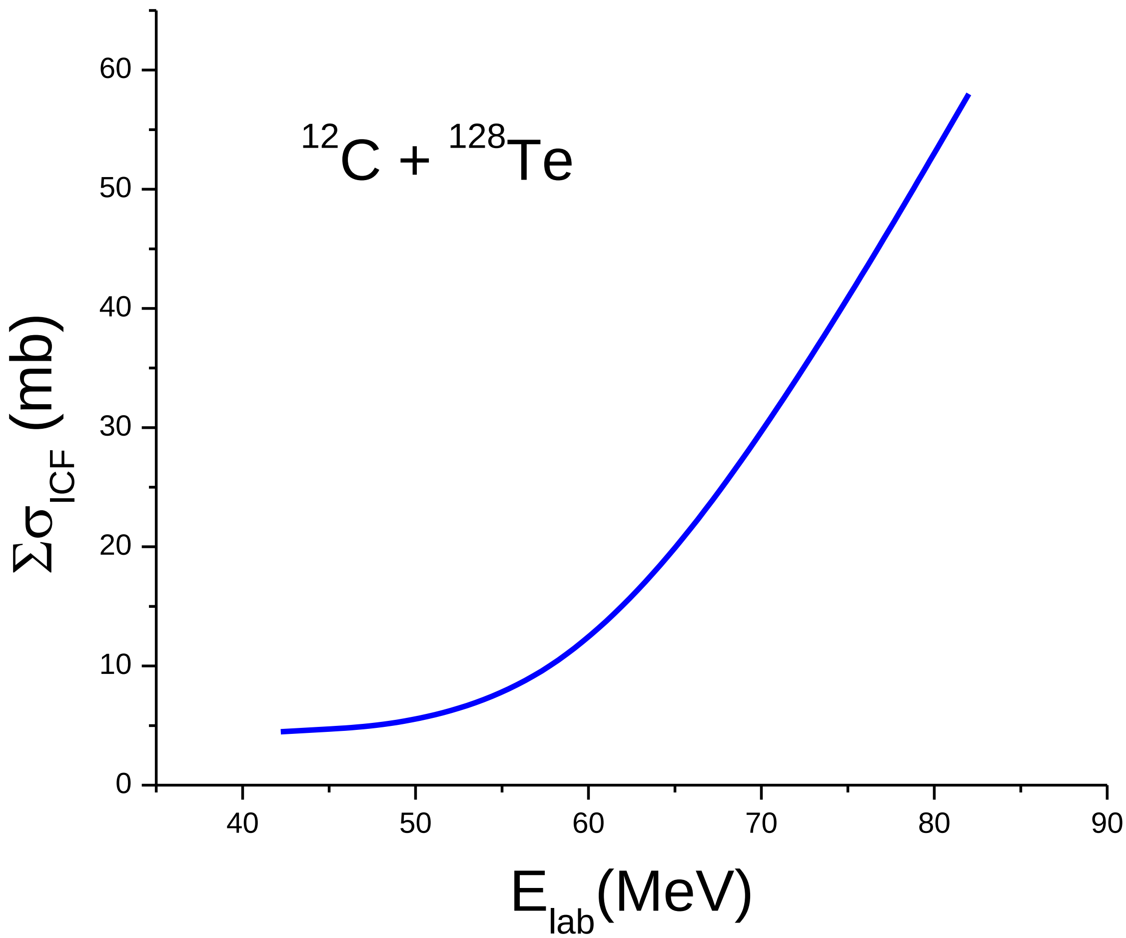

Figure 4.3: Deduced total ICF cross-section versus projectile energy in $^{12}C + ^{128}Te$ system.

b) $^{12}C + ^{141}Pr$ system

Similarly, in the $^{12}C + ^{141}Pr$ system, ^{148}Eu, ^{146}Sm, ^{143}Pm, ^{147}Eu, ^{146}Eu, ^{144}Sm, ^{142}Sm ^{142}Nd, ^{141}Nd, ^{145}Pm, ^{144}Pm, and ^{142}Pm residues are populated via CF and ICF reactions. The deduced total, incomplete fusion cross section is drawn in Figure 4.4 as a function of projectile energy. It may be observed from this figure that the deduced ICF cross-section, in general, increases with projectile energy, which is expected to increase as the break-up probability of the incident projectile significantly increases with projectile energy.

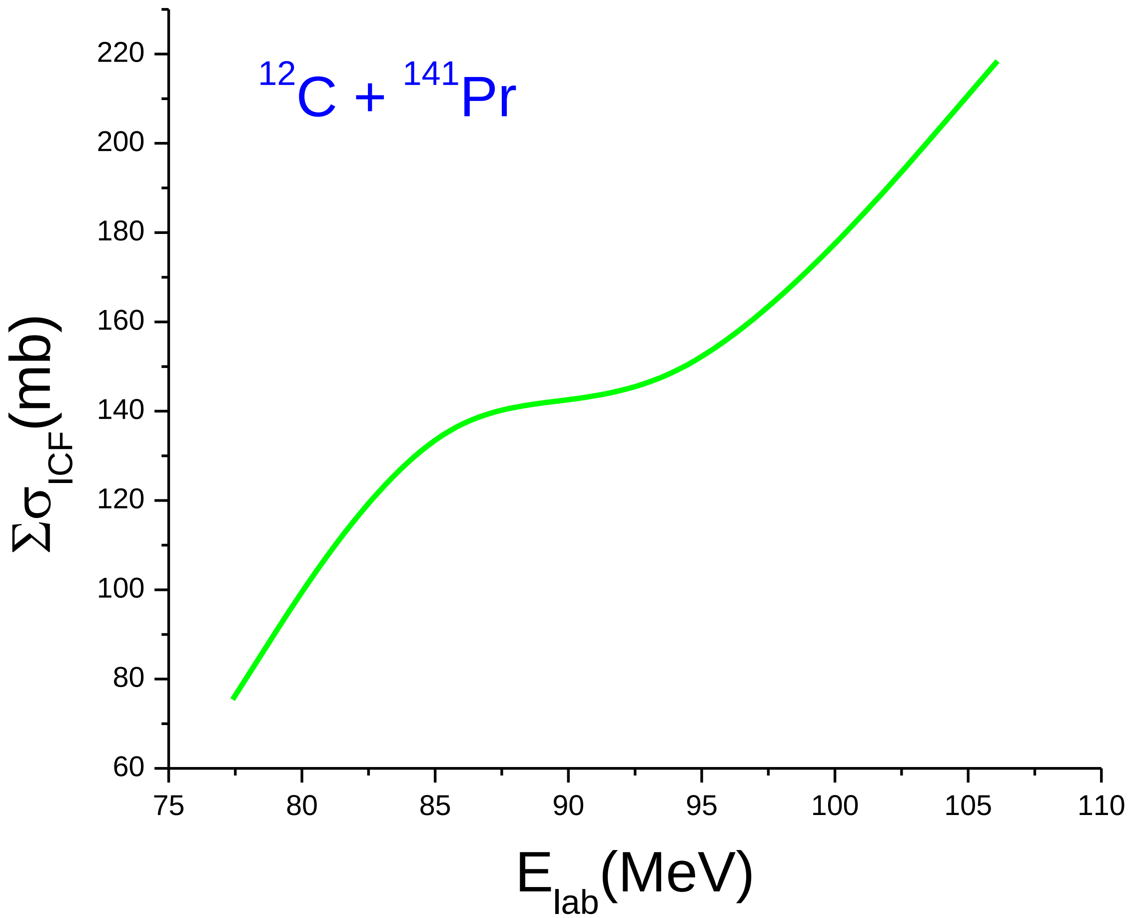

Figure 4.4: Deduced sum of ICF cross-section in $^{12}C + ^{141}Pr$ system as a function of projectile energy.

c) $^{12}C + ^{159}Tb$ system

In $^{12}C + ^{159}Tb$ system ^{165}Tm, ^{163}Tm, ^{161}Ho and ^{160}Ho residues are populated via CF and ICF reactions via (^{12}C, α2n), (^{12}C, α4n), (^{12}C, 2α2n) and (^{12}C, 2α3n) channels respectively. The deduced total, incomplete fusion cross section is drawn in Figure 4.5 as a function of projectile energy. As can be seen from this figure, as projectile energy increases, the contribution of ICF also increases.

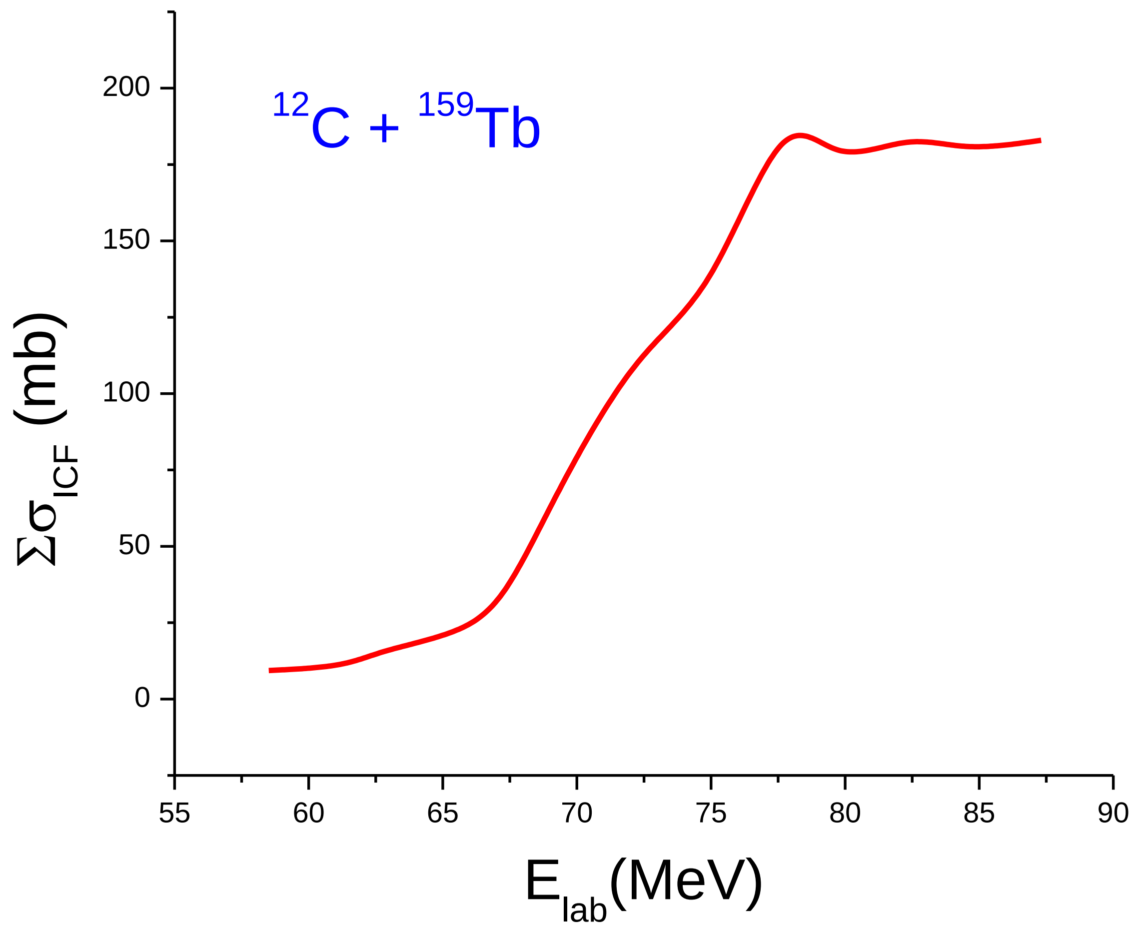

Figure 4.5: Deduced total ICF cross-section in ^{12}C + ^{159}Tb system as a function of projectile energy.

4.1.2. ^{16}O-induced reactions

In ^{16}O-induced projectile + target systems, we also follow the same procedures and approach we used for ^{12}C-induced reactions in selecting the best-fitted level density parameter values and deductions of ICF cross-section for individual channel and projectile + target systems.

a) ^{16}O + ^{130}Te system

In ^{16}O + ^{130}Te system ^{131}Xe, ^{133}Xe and ^{139}Ce residues are populated respectively through (^{16}O, 3α3n), (^{16}O, 3αn) and (^{16}O, α3n) channels. These reaction channels are populated through CF and ICF reaction during the interaction of ^{16}O projectile with ^{130}Te-target. Figure 4.6 shows the sum of the deduced ICF cross-section for the ^{16}O + ^{130}Te system. As can be seen from Figure 4.6, as projectile energy increases, the contribution of ICF also increases.

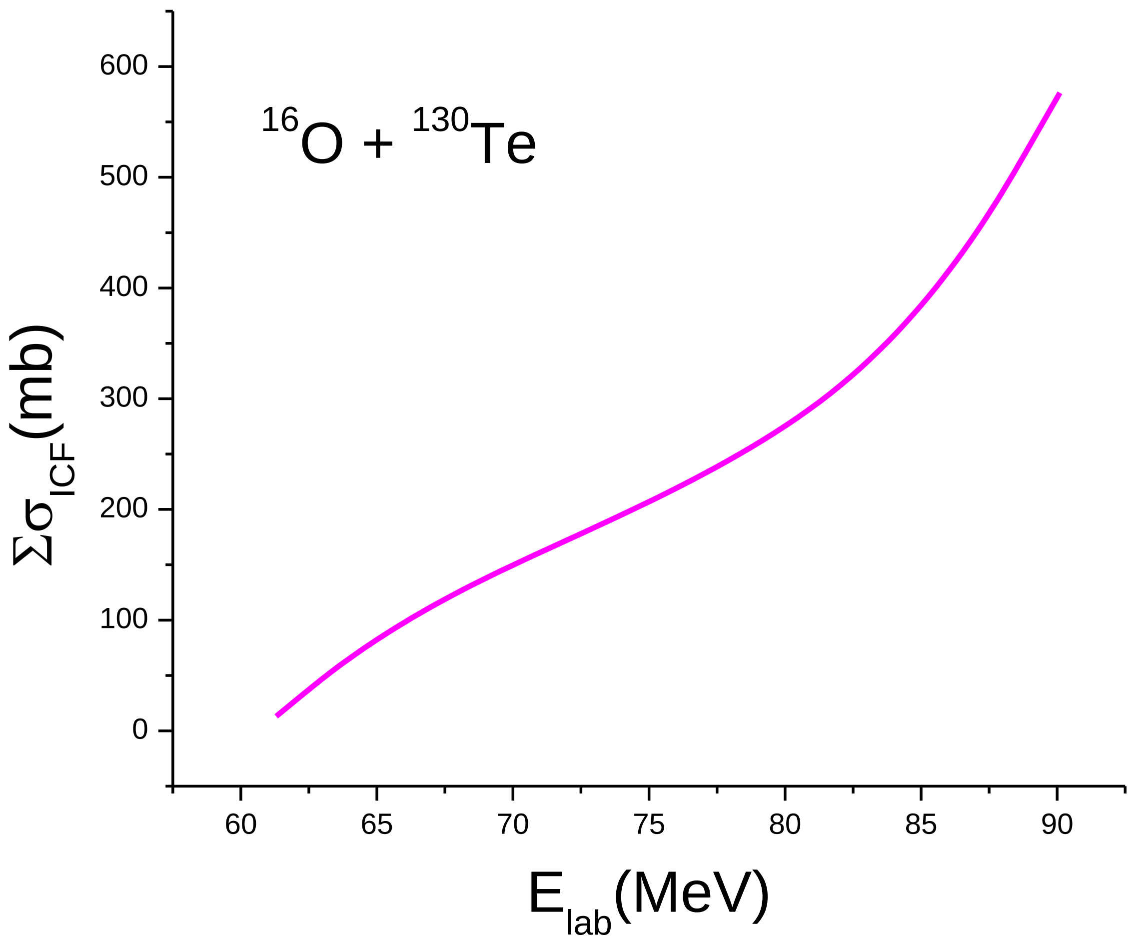

Figure 4.6: Deduced total ICF cross-section in ^{16}O + ^{130}Te system as a function of projectile energy.

b) $^{16}O + ^{159}Tb$ system

Similarly, in $^{16}O + ^{159}Tb$ system ^{167}Lu, ^{168}Lu, ^{166}Tm and ^{167}Yb residues are populated through (^{16}O, α4n), (^{16}O, α3n), (^{16}O, 2αn) and (^{16}O, αp3n) channels respectively. These reaction channels are populated through CF and ICF reactions during the interaction of the ^{16}O projectile with the ^{159}Tb target. Figure 4.7 shows the deduced total ICF cross-section, $\Sigma\sigma_{ICF}$, along with the projectile energy. This figure shows that the total incomplete fusion reaction cross-section in the $^{16}O + ^{130}Tb$ system increases with projectile energy.

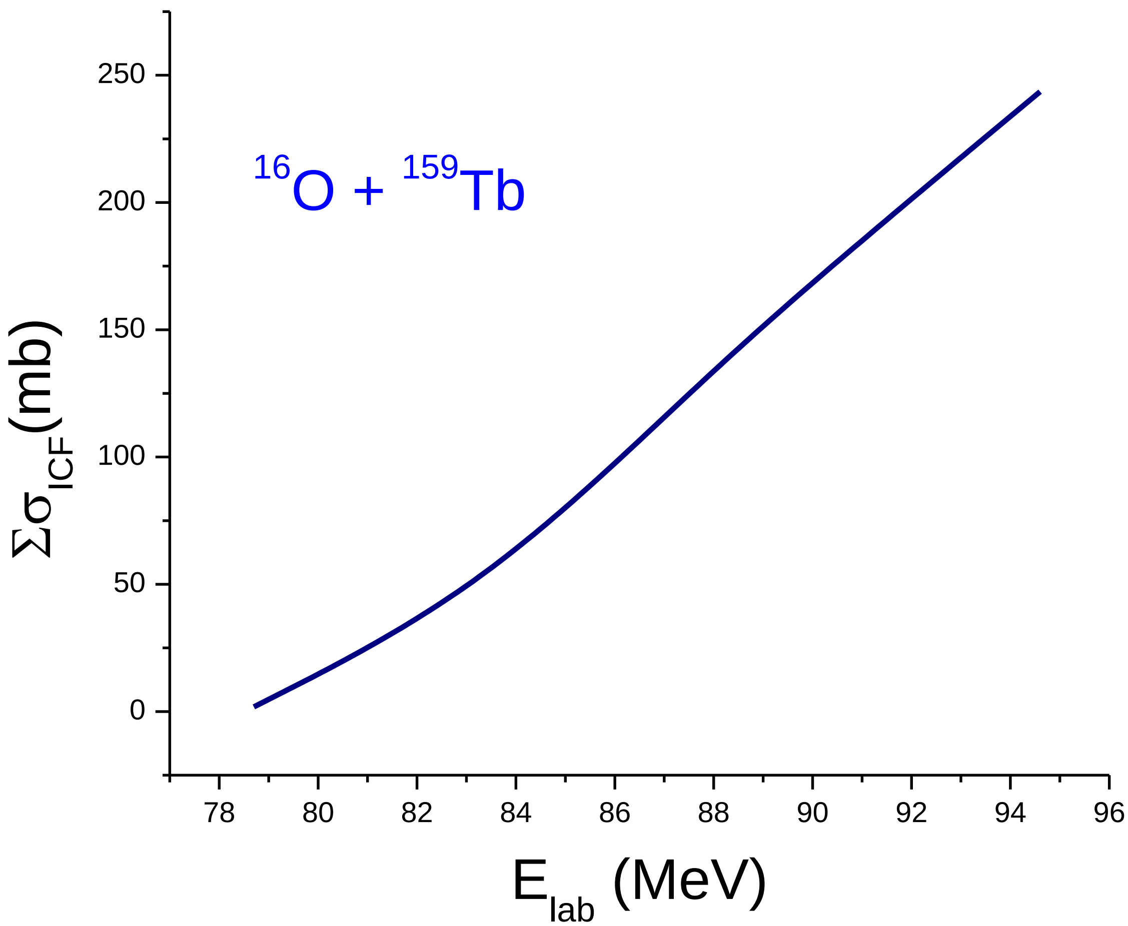

Figure 4.7: Deduced total ICF cross-section in $^{16}O + ^{159}Tb$ system as a function of projectile energy.

c) $^{16}O + ^{181}Ta$ system

In the same way, in $^{16}O + ^{181}Ta$ system ^{192}Au, ^{191}Au and ^{190}Au residues are respectively populated through (^{16}O, αn), (^{16}O, α2n) and (^{16}O, α3n) channels. These reaction channels are populated through CF and ICF reactions during the interaction of the ^{16}O projectile with the ^{181}Ta-target. Figure 4.8 shows the deduced total ICF cross-section, $\Sigma\sigma_{ICF}$, along with the projectile energy. As can be seen from this figure, the total, incomplete fusion reaction cross-section increases with projectile energy in the $^{16}O + ^{181}Ta$ system.

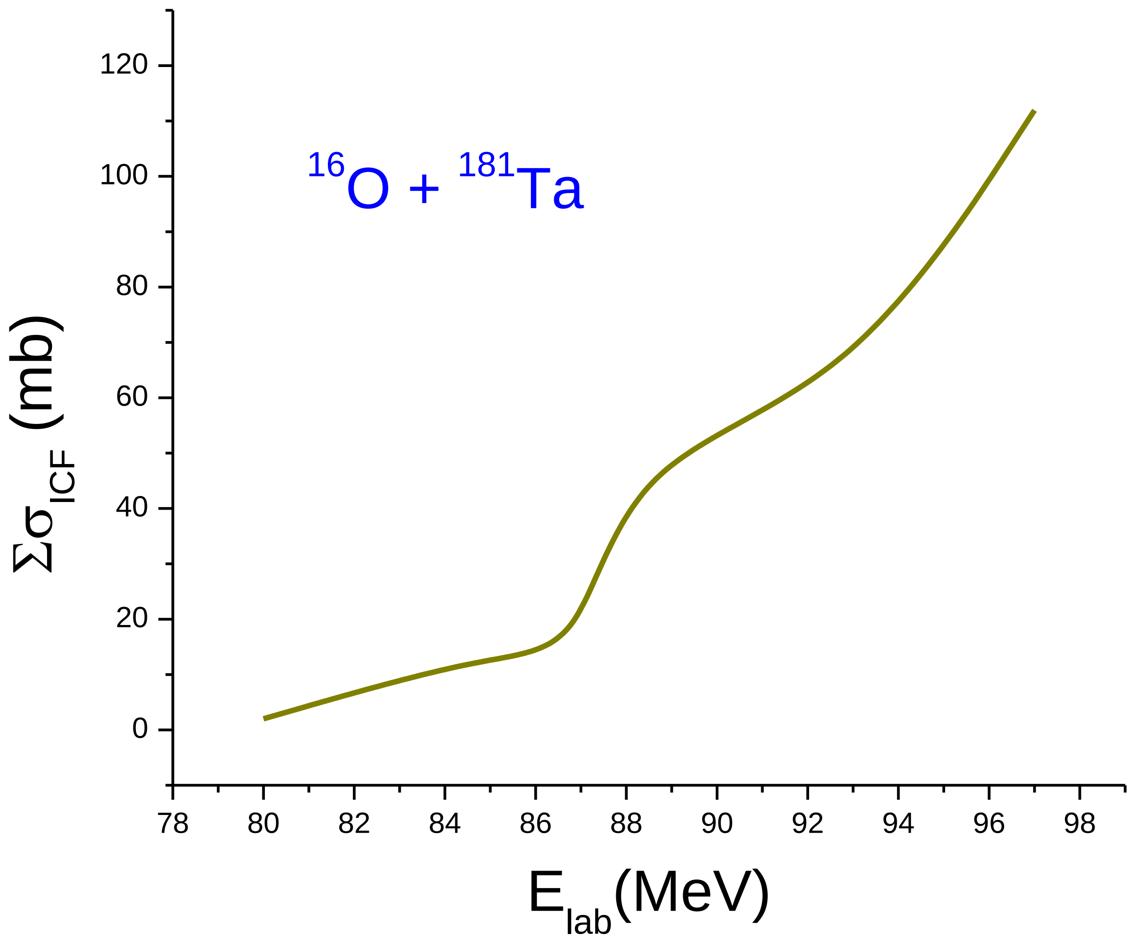

Figure 4.8: Deduced total ICF cross-section in $^{16}O + ^{130}Te$ system as a function of projectile energy.

In general, as Figure 4.9 shows, the total incomplete fusion reaction cross section in ^{12}C + ^{128}Te, ^{12}C + ^{141}Pr, ^{12}C + ^{159}Tb, ^{16}O + ^{130}Te, ^{16}O + ^{159}Tb, and ^{16}O + ^{181}Ta projectiles-targets systems, increases with normalized projectile energy.

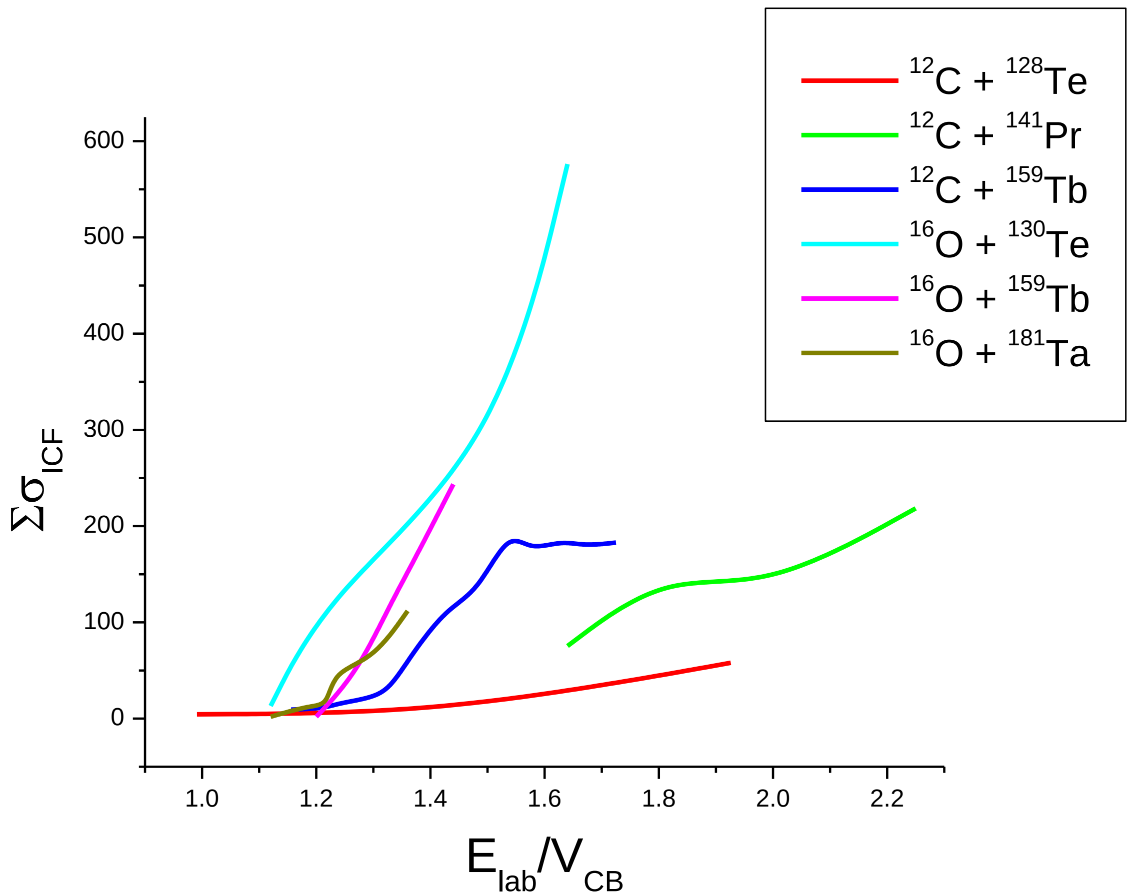

Figure 4.9: Deduced total ICF cross-section in ^{12}C + ^{128}Te, ^{12}C + ^{141}Pr, ^{12}C + ^{159}Tb, ^{16}O + ^{130}Te, ^{16}O + ^{159}Tb and ^{16}O + ^{181}Ta systems as function of normalized projectile energy.

4.2. The relative contribution of incomplete fusion

In this section, we tried to deduce the relative contribution of the incomplete fusion reaction on all fusion reactions using a quantity called incomplete fusion fraction, F_{ICF}, which represents the relative contribution of incomplete fusion cross section ($\Sigma\sigma_{ICF}$) from total fusion cross section (σ_{Total}=$\Sigma\sigma_{CF}$+ $\Sigma\sigma_{ICF}$). The percentage incomplete fusion contribution, F_{ICF} (%), is deduced using the following equation.

F_{ICF} (%) = $\frac{\Sigma\sigma_{ICF}}{\Sigma\sigma_{CF}+\Sigma\sigma_{ICF}} \times 100$ ……………… (4.1)

To see the correlation between projectile energy on ICF reaction, the value of the percentage incomplete fusion fraction, F_{ICF} (%) for ^{12}C + ^{128}Te, ^{12}C + ^{141}Pr, ^{16}O + ^{130}Te, ^{16}O + ^{159}Tb, and ^{16}O + ^{181}Ta projectile-target systems were plotted as a function of normalized projectile energy (E_{lab} /V_{CB}), E_{lab} /V_{CB} used to absorb the impact of the coulomb barrier ($V_{CB} = \frac{Z_P Z_T}{\sqrt[3]{A_P}+\sqrt[3]{A_T}}$) from different projectile-target systems.

Figure 4.10 shows the percentage ICF fraction, F_{ICF} (%), as a function of normalized projectile energy, E_{lab} /V_{CB}, for presently investigated projectile + target systems.

As the figure shows for both ^{12}C and ^{16}O-induced projectile + targets systems, the contribution of incomplete fusion generally increases with an increase in the normalized projectile energy.

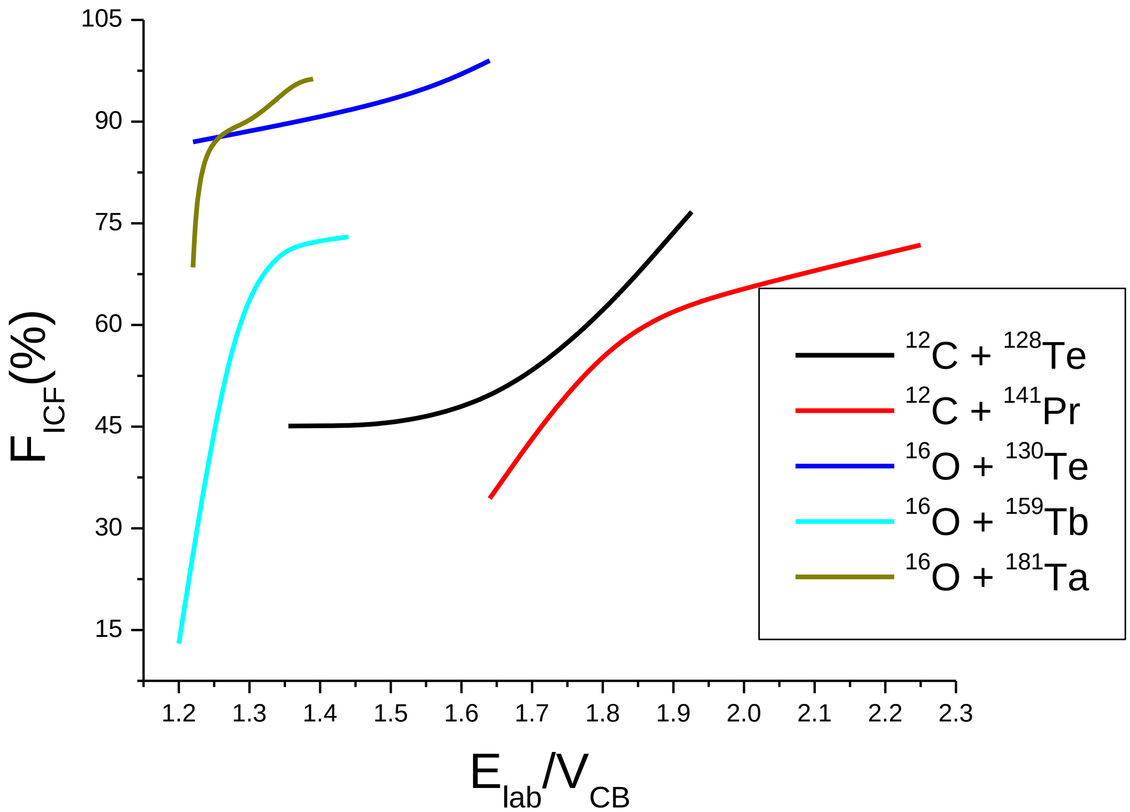

Figure 4.10: Percentage ICF fraction, as a function of normalized projectile energy for ^{12}C + ^{128}Te, ^{12}C + ^{141}Pr, ^{16}O + ^{130}Te, ^{16}O + ^{159}Tb, and ^{16}O + ^{181}Ta systems.

Furthermore, in this work, to see the impact of entrance channel mass-asymmetry ($M_a = \frac{A_T}{A_T+A_P}$) on the ICF reaction, the deduced values of F_{ICF} (%) are plotted as a function of normalized relative velocity (${V_{rel}}/{c}$). ${V_{rel}}/{c}$ is used here to absorb the difference in coulomb barrier between different projectile-target systems and is given by:

$$ {V_{rel}}/{c} = \sqrt{\frac{2(E_{CM}-V_{CB})}{\mu c^2}} \quad \ldots\ldots\ldots\ldots\ldots\ldots (4.2)$$

E_{CM} represents the center of mass energy, $E_{CM} = \frac{A_T}{A_T+A_P} E_P$, and μ is the reduced mass of the system, $\mu = \frac{A_P\, A_T}{A_T+A_P}$.

Figures 4.11, 4.12, and 4.13 displayed a graph of the percentage ICF fraction, F_{ICF} (%) versus normalized relative velocity, $V_{rel}/_{c}$ for three paired $^{12}C + ^{159}Tb - ^{12}C + ^{128}Te$, $^{12}C + ^{159}Tb - ^{12}C + ^{141}Pr$ and $^{16}O + ^{159}Tb - ^{16}O + ^{181}Ta$ projectile-target systems that have at least one the same normalized projectile energy points so that we can obtain a clear association between F_{ICF} and entrance channel mass-asymmetry. Mass asymmetry ($M_a = \frac{A_T}{A_T + A_P}$) of $^{12}C + ^{159}Tb$, $^{12}C + ^{128}Te$, $^{12}C + ^{141}Pr$, $^{16}O + ^{159}Tb$ and $^{16}O + ^{181}Ta$ projectiles + targets systems are ≈ 0.9298amu, 0.9143amu, 0.9216amu, 0.9068amu and 0.9188amu respectively.

Figure 4.11 shows that at v_{rel} ≈ 0.044c, the percentage of incomplete fusion fraction are ≈ 55.6 and 45.1 for $^{12}C + ^{159}Tb$ and $^{12}C + ^{128}Te$ systems respectively, Also, at v_{rel} ≈ 0.066c, the percentage of incomplete fusion fraction of $^{12}C + ^{159}Tb$ system and $^{12}C + ^{128}Te$ system are ≈ 79.9 and 45.3 respectively. This figure show that percentage of incomplete fusion fraction of $^{12}C + ^{159}Tb$ (Ma≈0.9298amu) system is higher than $^{12}C + ^{128}Te$ (Ma≈0.9143amu) system.

Similarly, figure 4.12 show that at the same relative velocity, percentages of incomplete fusion fraction are ≈ 79.9 and 34.4 for $^{12}C + ^{159}Tb$ (Ma≈0.9298amu) and $^{12}C + ^{142}Pr$ (0.9216amu) systems respectively. It indicated that percentage of incomplete fusion fraction is higher for mass asymmetric projectile + target system.

In the same way, figure 4.13 show that at the same relative velocity (≈0.03c, 0.045c and 0.05c), percentage of incomplete fusion reaction of $^{16}O + ^{181}Ta$ (0.9188amu) system is higher than $^{16}O + ^{159}Tb$ (0.9068amu) system.

As can be seen from these figures, the contribution of ICF reaction at the same relative velocity (vertical lines), in general, is higher for the mass-asymmetric system than the symmetric system. Furthermore, the result suggested that the probability of ICF reaction is higher for a mass-asymmetric system, which is consistent with the findings of Morgenstern et al. [20].

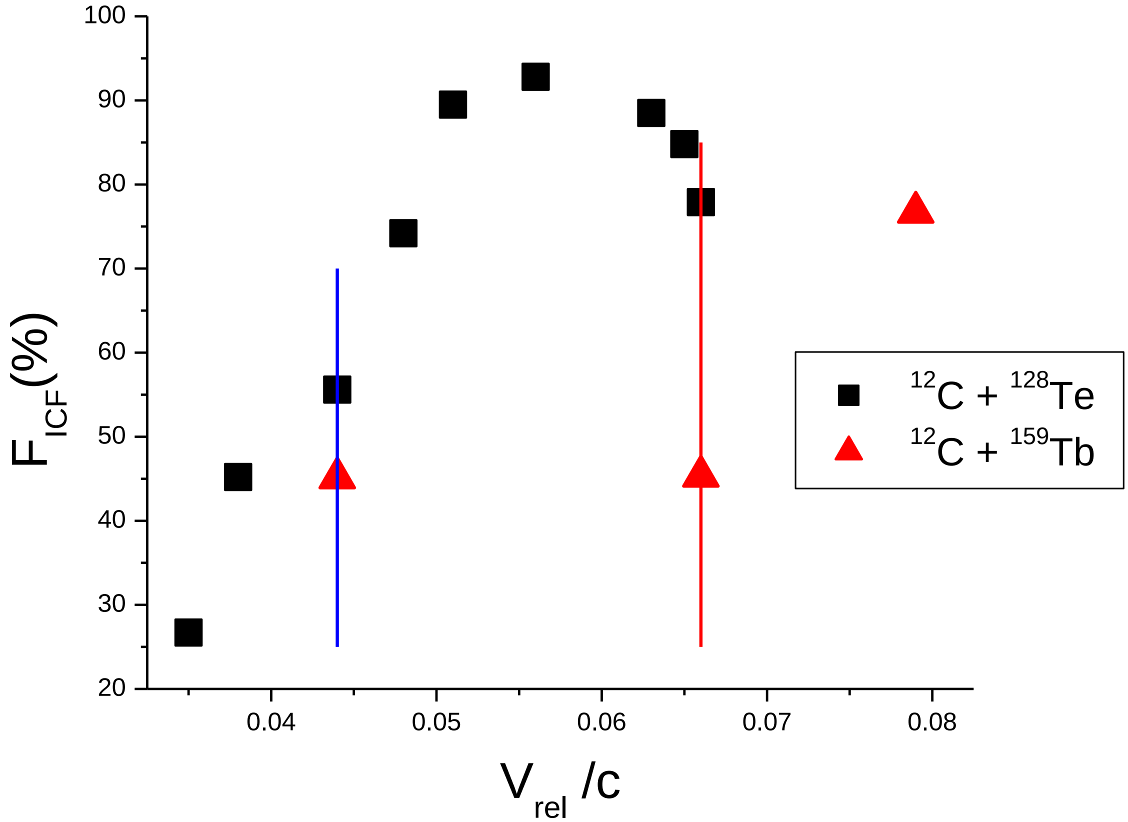

Figure 4.11: Percentage ICF fraction versus normalized relative velocity for $^{12}C + ^{159}Tb$ – $^{12}C + ^{128}Te$ pair of systems.

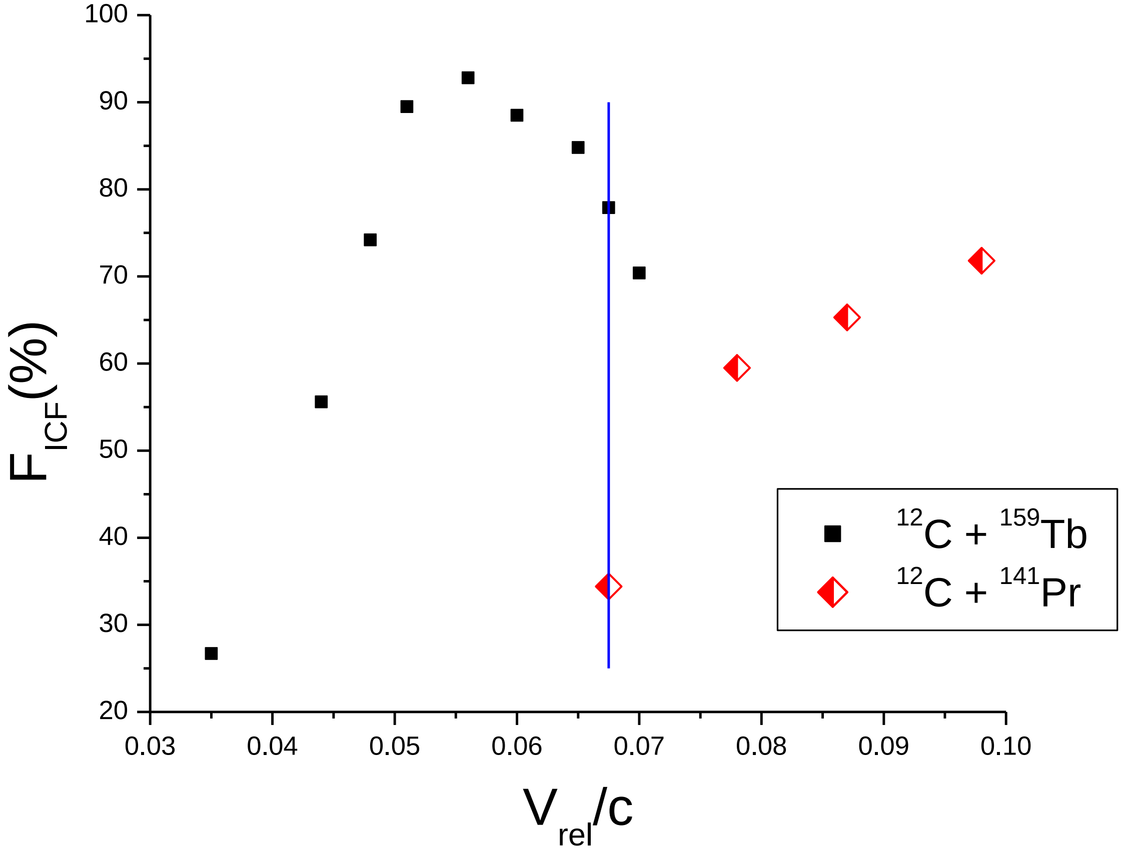

Figure 4.12: Percentage ICF fraction versus normalized relative velocity for $^{12}C + ^{159}Tb$ – $^{12}C + ^{141}Pr$ pair of systems.

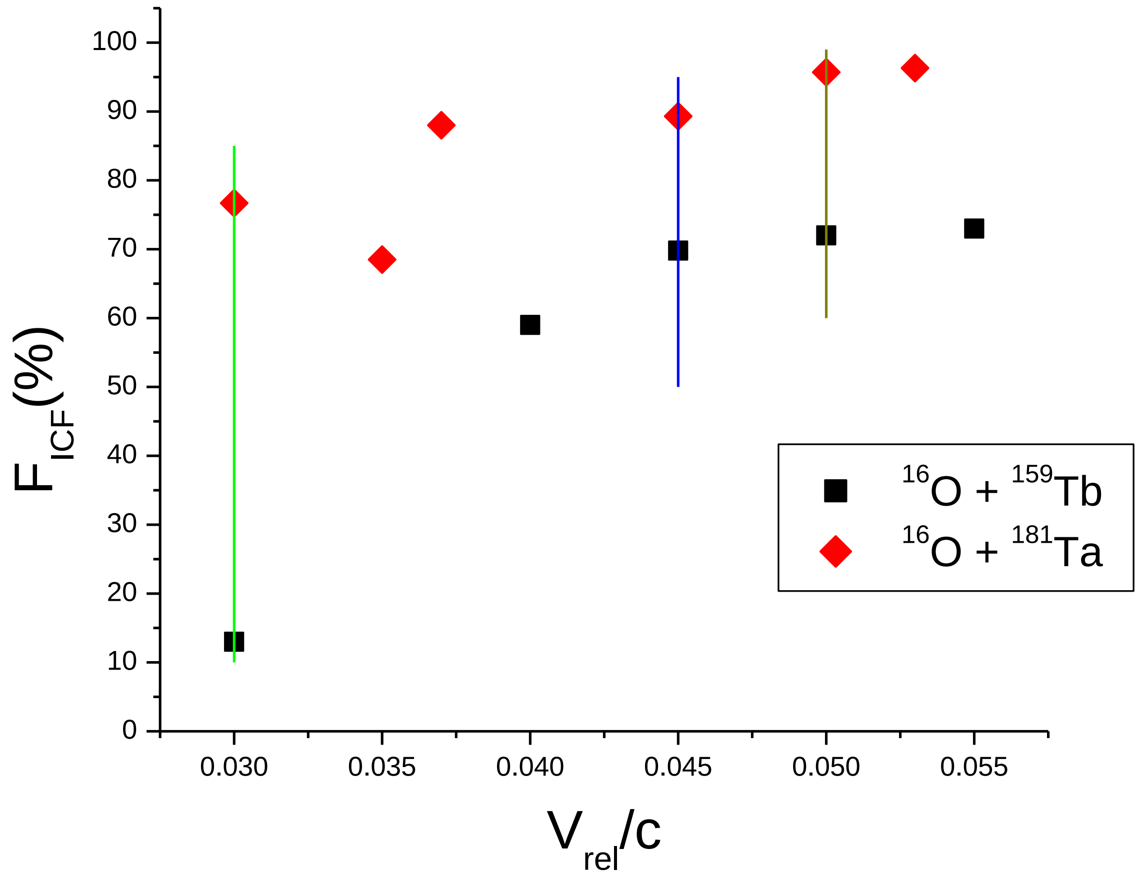

Figure 4.13: Percentage ICF fraction versus normalized relative velocity for $^{16}O + ^{159}Tb$ – $^{16}O + ^{181}Ta$ pair of systems.

CHAPTER FIVE

5. SUMMARY AND CONCLUSION

In the present work, to study the incomplete fusion reaction correlation with projectile energy and mass asymmetry, the excitation functions of α-emitting and non-α-emitting channels in ^{12}C + ^{128}Te, ^{12}C + ^{141}Pr, ^{12}C + ^{159}Tb, ^{16}O + ^{130}Te, ^{16}O + ^{159}Tb and ^{16}O + ^{181}Ta systems have been examined in the framework of statistical model code PACE4 at ≈ 3-9 MeV/nucleon. For a representative non-α-emitting (^{12}C, 4n) channel from a representative in ^{12}C + ^{159}Tb system, experimentally measured cross sections agreed with PACE4 prediction for level density parameters K=10. For the same level density parameters a representative α-emitting (^{12}C, α3n) channel from a representative in ^{12}C + ^{128}Te projectile + target system, the experimentally measured cross sections are higher than the PACE4 predicted. The observed difference is attributed to the contribution of incomplete fusion following the prompt break-up of the projectile into α-clusters.

It was found that the incomplete fusion reaction generally increases with increasing projectile energy. Furthermore, the results indicated that at the same normalized relative velocity, incomplete fusion fraction is higher for mass-asymmetric projectile + target systems.

Thus, an incomplete fusion reaction is sensitive to the projectile energy and the entrance channel mass-asymmetry.

REFERENCE

1. D. Sing, Pankaj K. Giri, Amritraj Mahato, Sneha B.Lida, Harish Kumar, M. Afzal Ansari, Rahbar Ali, Suhail A.Tali, M.H.Rashid, R. Guin, and S.K.Das. (2019) Probing of incomplete fusion dynamics and its correlation with various systematic. Nuclear physics A, volume 981, pages 75-88.
   https://www.sciencedirect.com/science/article/pii/S0375947418303671.
2. F. K. Amanuel, B. Zelalam, A. K. Chaubey, Avinash Agarwal, I.A. Risvi, Anjana Maheshwari and Tauseef Ahmed. (2011). Investigation of the influence of incomplete fusion on complete fusion of ^{12}C-induced reactions at 4-7.2 MeV/nucleon.
   Eur. Phys. J. A 47:156.
3. P.P. Singh, R. Kumar, B.P. Singh, M.K. Sharma, Unnati, D.P. Singh, R. Prasad, K.S. Golda,(2008) Phys. Rev. C 77, 014607 .
4. Suhail A. Tali, Harish Kumar, M. Afzal Ansari, Asif Ali, D.Singh, Rahbar Ali, Pankaj K. Giri, Sneha B.Linda, Siddharth Parashari, R. Kumar, R.P. Singh, S. Muralithar.(2018). Study of incomplete fusion reaction dynamics in ^{13}C+ ^{165}Ho systems and its dependence on various entrance channel parameters. NuPhA.970..208T.
   https://doi.org/10.016/j.nuclphysa.2017.11.012.
5. Rahbar Ali, D Singh, Suhail A Tali, Harish Kumar, Mohd Asif Khan, Nitin Sharma, Jagat Jyoti Mohapatra, Lupteindu Chhura, M Afzal Ansari, M H Rashid, R Guin, S K Das, Rakesh Kumar and S Muralithar. (2023). Systematic study of Incomplete Fusion Dynamics with Various Entrance Channel Parameters. Indian Journal of Pure & Applied Physics Vol. 61, pp. 697-703
   DOI:10.56042/ijpap.v61i8.1327.
6. H.C. Britt, A.R Quinton, (1961) Phys. Rev. 124,877.
7. T. Inamura, M. Ishihara, T. Fakuda, T. Shimoda, H. Hiruta, (1977) Phys. Lett. B 68, 51.
8. Vijay R Sharma, Mohd. Shuaib, Pushpendra P. Singh, Abhishek Yadav, Manoj K. Sharma, R. Kumar, B. P. Singh, S. Muralithar, R. P. Singh, R. K. Bhowmik and R. Prasad.(2018)
   IOP Conf. Series: Journal of Physics: Conf. Series 1078 012020. Doi: 10.1088/1742-6596/1078/1/012020.

9. Sunil Dutt, Avinash Agarwal, Munish Kumar, Vijay R. Sharma, I. A. Rizvi, R. Kumar, and A. K. Chaubey. (2014) Mass-Asymmetry effects in heavy ion reactions: Complete fusion Vs incomplete fusion. http://dx.doi.org/10.1051/epjconf/20146603024.
10. T. Udagawa and T. Tamura, (1980) Phys. Rev. Lett. 45, 1311.
11. J.Wilczynski,K.Siwek-Wilczynska,J.VanDriel,S.Gonggrijp, D. C. J. M. Hageman, R. V. F. Janssens, J. Lukasiak, R. H. Siemssen, and S. Y. Van Der Werf,(1982) Nucl. Phys. A 373, 109.
12. Pushpendra P. Singh , B.P. Singh, M.K. Sharma , Unnati Gupta , Rakesh Kumar , D. Singh , R.P. Singh ,S. Murlithar , M.A. Ansari , R. Prasad , R.K. Bhowmik, (2009) Physics Letters B 671 20–24.
13. N.Wang, X.Wu, Z.Li, M.Liu, and W.Scheid, (2006) Phys.Rev.C74, 044604.
14. M. Blann, (1971) Phys. Rev. Lett. 27, 337.
15. R. Weiner et al., (1980) Nucl. Phys. A 286, 282.
16. J.P. Bondrof, J.N.De, G.Fai, A.O.T.Karvinen, and J.Randrup, (1980) Nucl. Phys. A 333, 285.
17. V. I. Zagrebaev, (1990) Ann. Phys. (NY) 197, 33.
18. Ali et al. (2023) Systematic Study of Incomplete Fusion Dynamics with Various Entrance Channel Parameters, Indian Journal of Pure & Applied Physics, Vol. 61, pp. 697-703.
19. Pavneet Kaur, Moumita Maiti, T.N.Nag, S.Sodaye, (2022) phys. Rev. C 105, 014629.
20. H. Morgenstern, W. Bohne, W. Galster, K. Grabisch, A. Kyanowski,(1984) Phys. Rev. Lett. 52, 1104.
21. W.N. Cottingham, D.A. Green Wood. (2004) An Introduction to Nuclear Physics, Cambridge University, press. Chapter 8.
22. Shiken. Physics conservation law. https://shiken.ai/physics/conservation-laws.
23. Anwar Kamal. (2014) Nuclear physics. Murphy, TX, USA. Graduate texts in physics. www.springer.com/series/8431. Chapter 7.
24. Krane K. S, John wiley, (1987). Introductory nuclear physics. Chapter 11.
25. V.K. Mittal, R.C. Verma, S.C. Gupta. (2013) Introduction to Nuclear and Particle Physics, Raj press, New Delhi-110012. Chapter 4.
26. Cources.washington.edu>handouts: cross section.
27. P E Hodgson. (1987) Rep. Prog. Phys. 50. 1171-1228.

28. P E Hodgson. (1972) Direct and Compound Processes in Nuclear Reactions. Phys. Vol. 2, N.^{0} 1.
29. A. Klimov, (1975) Nuclear physics and nuclear reactions MIR Publishers. Moscow. Chapter 3, page 143.
30. B.B. Back, H. Esbensen, C. L. Jiang, and K. E. Rehm. (2014). Recent developments in heavy-ion fusion reactions. Rev. Mod. Phys., Vol. 86, No. 1.
31. J. Rangela, M.R. Cortesa, J. Lubiana, L.F. Cantob. (2020) Physics Letters B 803 135337.
32. E.A. Bakkum, P. Decowski, K.A. Griffioen, R.J. Meijer, R. Kamermans, (1989) Phys. Rev. C 39, 2094.
33. Avinash Agarwal , Anuj Kumar Jashwal, Munish Kumar, and S. Prajapati, Sunil Dutt, Muntazir Gull, and I. A. Rizvi, Kamal Kumar, Sabir Ali, Abhishek Yadav, R. Kumar, A. K. Chaubey.(2022) Physical Review C 105, 034609.
34. Siwek-Wilczyńska K, du Marchie van Voorthuysen E H, van Popta J, Siemssen R H and Wilczyński J (1979). Phys. Rev. Lett. 42 1599.
35. Bhushan Bhujang, Pragya Das, R P Singh, R Tripathi and B S Tomar (2013) J. Phys.: Conf. Ser. 420 012128.
36. Bondorf J P, De J N, Karvien A 0 T. Fi G and Jacobson B (1979) Phys. Lett, 84B 162-5.
37. H Fuchs and K Mohring (1994) Rep. Bog. Phys. 57 231-324.
38. B.G. Harvey and H. Homeyer (1983). An overlap model for fragment yields in heavy ion reactions. https://escholarship.org/uc/item/2m85x31m.
39. A.Gavron, (1980) Phys. Rev. C21 230-236; (ftp://ftp.nscl.msu.edu/lise/PACE_source).
40. F. K. Amanuel, B. Zelalem, A. K. Chaubey, Avinash Agarwal, I. A. Rizvi, Anjana Maheshwari, and Tauseef Ahmed.(2011) Role of break-up processes in the fusion of the 12C+ 52Cr system. Physical Review C 84, 024614.
41. Manoj Kumar Sharma, B.P. Singh, Sunita Gupta, M.M. Muthafa, H.D. Bhardwaj, R. Prasad, A.K. Sinha, (2003) J. Phys. Soc. Jpn. 72, 1917.
42. R. Kossakowski, J.Jastrzebski, P.Rymuza, A.Gizon, S.Andre, J.Genevey, J.Gizon, V.Barci, (1985) physical review C vol. 32 no. 5.
43. Abhishek Yadav, Vijay R. Sharma, Pushpendra P. Singh, Devendra P. Singh, Manoj K. Sharma, Unnati Gupta, R. Kumar, B. P. Singh, R. Prasad, and R. K. Bhowmik, (2012) Physical Review C 85, 034614.

44. Devendra P. Singh, Vijay R. Sharma, Abhishek Yadav, Pushpendra P. Singh, Unnati, M. K. Sharma, R. Kumar, B. P. Singh, R. Prasad, (2014) Physical Review C 89, 024612.
45. Pushpendra P. Singh, B. P. Singh, Manoj Kumar Sharma, Unnati, Devendra P. Singh, R. Prasad, Rakesh Kumar, K. S. Golda, (2008) Physical Review C 77, 014607.
46. Devendra P. Singh, Unnati, Pushpendra P. Singh, Abhishek Yadav, Manoj Kumar Sharma, B. P. Singh, K. S. Golda, Rakesh Kumar, A. K. Sinha, R. Prasad, (2009) Physical Review C 80, 014601.
47. S. M. Grimes (2013) Physical Review C 88, 024613.

Data Tables

1. $^{12}C+^{128}Te$ system

Energy (MeV)	$^{133}Ba(\alpha 3n)$			$^{131}Ba(\alpha 5n)$			$^{131}Te(\alpha 4pn)$			$\Sigma\sigma_{TF}$ (mb)	$\Sigma\sigma_{ICF}$ (mb)	E_{lab}/V_{CB}
	σ_{expr} (mb)	σ_{CF} (mb) PACE4 K=10	σ_{ICF} (mb)	σ_{expr} (mb)	σ_{CF} (mb) PACE4 K=10	σ_{ICF} (mb)	σ_{expr} (mb)	σ_{CF} (mb) PACE4 K=10	σ_{ICF} (mb)			
42.2	0.08	-	0.08	-	-		4.4	-	4.4	4.48	4.48	0.991
57.7	7.8	6.97	0.83	-	-		4.9	-	4.9	12.7	5.73	1.355
70.8	43.6	36.4	7.2	0.73	0.0116	0.72	22.2	-	22.2	66.53	30.12	1.663
82	37.6	10.5	27.1	7.1	15.8	-	30.9	-	30.9	75.6	58	1.926

Table 1.1; experimentally measured production cross sections (σ_{expr}), theoretically reproduced cross section (σ_{CF}) and calculated ICF cross section of ^{133}Ba, ^{131}Ba and ^{131}Te residues along with $\Sigma\sigma_{TF}$, $\Sigma\sigma_{ICF}$ and E_{lab}/V_{CB}.

Energy (MeV)	V_{rel}/c	F_{ICF}
42.2	-	1
57.7	0.045	0.451
70.8	0.066	0.453
82	0.079	0.767

Table 1.2 Normalized relative velocity and incomplete fusion reaction of $^{12}C+^{128}Te$ system.

2. $^{12}C + ^{141}Pr$ system

Energy (MeV)	^{143}Pm (2α2n)			^{146}Eu (α3n)			^{147}Eu (α2n)			^{142}Sm (αp6n)		
	σ_{expr} (mb)	σ_{CF} (mb) PACE4 K=10	σ_{ICF} (mb)	σ_{expr} (mb)	σ_{CF} (mb) PACE4 K=10	σ_{ICF} (mb)	σ_{expr} (mb)	σ_{CF} (mb) PACE4 K=10	σ_{ICF} (mb)	σ_{expr} (mb)	σ_{CF} (mb) PACE4 K=10	σ_{ICF} (mb)
77.4	15	10.3	4.7	124	152	-	45	3.58	41.42	-	-	-
85.5	31	8.62	22.38	119	59.9	59.1	19	0.289	18.71	-	-	-
93.8	45	2.06	42.94	75	8.86	66.14	-	-	-	-	-	-
106.1	45	0.656	44.341	45	4.31	40.69	21	7.81	13.19	23	0.088	22.91

Table 2.1 Experimentally measured production cross sections (σ_{expr}), Theoretically reproduced cross section (σ_{CF}) and calculated ICF cross section of ^{143}Pm, ^{146}Eu, ^{147}Eu and ^{142}Sm residue in $^{12}C+^{141}Pr$ system.

Energy (MeV)	^{144}Sm (αp4n)			^{142}Nd (2αp2n)			^{141}Nd (2αp3n)			^{142}Pm (2α3n)		
	σ_{expr} (mb)	σ_{CF} (mb) PACE4 K=10	σ_{ICF} (mb)	σ_{expr} (mb)	σ_{CF} (mb) PACE4 K=10	σ_{ICF} (mb)	σ_{expr} (mb)	σ_{CF} (mb) PACE4 K=10	σ_{ICF} (mb)	σ_{expr} (mb)	σ_{CF} (mb) PACE4 K=10	σ_{ICF} (mb)
77.74	-	-		-	-	-	-	-	-	-	-	-
85.5	12	0.74	11.26	-	-	-	-	-	-	24	15.8	8.2
93.8	19	18.9	0.1	-	-	-	-	-	-	23	27.9	-
106.1	49	62.9	-	23	1.47	21.53	13	4.7	8.3	36	12.5	23.5

Table 2.2 Experimentally measured production cross sections (σ_{expr}), Theoretically reproduced cross section (σ_{CF}) and calculated ICF cross section of ^{144}Sm, ^{142}Nd, ^{141}Nd and ^{142}Pm residue in $^{12}C+^{141}Pr$ system.

Energy (MeV)	^{144}Pm (2αn)			^{145}Sm (αp3n)			^{146}Sm (αp2n)			^{143}Eu (α6n)		
	σ_{expr} (mb)	σ_{CF} (mb) PACE4 K=10	σ_{ICF} (mb)	σ_{expr} (mb)	σ_{CF} (mb) PACE4 K=10	σ_{ICF} (mb)	σ_{expr} (mb)	σ_{CF} (mb) PACE4 K=10	σ_{ICF} (mb)	σ_{expr} (mb)	σ_{CF} (mb) PACE4 K=10	σ_{ICF} (mb)
77.74	23	0.475	22.525	-	-	-	7	5	2	-		
85.5	12	0.171	11.829	12	11.6	0.4	8	4.17	3.83	-		
93.8	-	-	-	19	17.9	1.1	-	-	-	23	0.098	22.90
106.1	-	-	-	49	5.03	43.97	-	-	-	65	71.2	-

Table 2.3 Experimentally measured production cross sections (σ_{expr}), Theoretically reproduced cross section (σ_{CF}) and calculated ICF cross section of ^{144}Pm, ^{145}Sm, ^{146}Sm and ^{143}Eu residue in ^{12}C+^{141}Pr system.

Energy (MeV)	^{148}Eu (αn)			$\Sigma\sigma_{TF}$ (mb)	$\Sigma\sigma_{ICF}$ (mb)	E_{lab}/V_{CB}	V_{rel}/c	F_{ICF}
	σ_{expr} (mb)	σ_{CF} (mb) PACE4 K=10	σ_{ICF} (mb)					
77.74	5	0.17	4.83	219	75.421	1.64	0.068	0.344
85.5	17	1.51	15.49	254	151.203	1.81	0.078	0.595
93.8	-	-	-	204	133.182	1.99	0.087	0.653
106.1	-	-	-	304	218.43	2.25	0.098	0.718

Table 2.4 Experimentally measured production cross sections (σ_{expr}), Theoretically reproduced cross section (σ_{CF}) and calculated ICF cross section of ^{148}Eu along with $\Sigma\sigma_{TF}$,$\Sigma\sigma_{ICF}$, E_{lab}/V_{CB}, V_{rel}/c and F_{ICF}.

3. $^{12}C+^{159}Tb$ system

Energy (MeV)	$^{165}Tm(\alpha 2n)$			$^{163}Tm(\alpha 4n)$			$^{161}Ho(2\alpha 2n)$		
	σ_{expr} (mb)	σ_{CF} (mb) PACE4 K=10	σ_{ICF} (mb)	σ_{expr} (mb)	σ_{CF} (mb) PACE4 K=10	σ_{ICF} (mb)	σ_{expr} (mb)	σ_{CF} (mb) PACE4 K=10	σ_{ICF} (mb)
58.51	13.66	7.3	6.36	-	-	-	-	-	-
61.37	16.65	12.2	4.45	-	-	-	-	-	-
62.63	19.61	11.3	8.31	1	-	1	-	-	-
65.49	17.45	11.3	6.15	8	0.0138	7.9862	-	-	-
67.24	12.52	8.81	3.71	22	0.0757	21.9243	-	-	-
69.15	10.16	6.71	3.45	58.41	0.455	57.955	1.37	0.141	1.229
72.24	8.76	4.27	4.49	108.17	3.91	104.26	4.49	0.483	4.007
74.97	8.21	2.39	5.82	129.68	13.8	115.88	6.25	0.587	5.663
77.77	8.98	0.848	8.132	202.54	32.5	170.04	7.5	0.576	6.924
79.62	9.98	0.817	9.163	189.9	45.2	144.7	6.34	0.817	5.523
82.42	12.04	0.264	11.776	211.26	67.5	143.76	5.31	0.924	4.386
84.44	17.79	0.199	17.591	204.1	80.8	123.3	4.5	0.522	3.978
87.31	18.9	0.363	18.537	212.23	90.3	121.93	2.1	0.506	1.594

Table 3.1 experimentally measured production cross sections (σ_{expr}), theoretically reproduced cross section (σ_{CF}) and calculated ICF cross section of ^{165}Tm, ^{163}Tm and ^{161}Ho residues in $^{12}C+^{159}Tb$ system

Energy (MeV)	^{160}Ho(2α3n)			$\Sigma\sigma_{TF}$ (mb)	$\Sigma\sigma_{ICF}$ (mb)	E_{lab}/V_{CB}	V_{rel}/c	F_{ICF}
	σ_{expr} (mb)	σ_{CF} (mb) PACE4 K=10	σ_{ICF} (mb)					
58.51	-	-	-	13.66	6.36	1.156	0.027	0.466
61.37	-	-	-	16.65	4.45	1.213	0.035	0.267
62.63	-	-	-	20.61	9.31	1.238	0.038	0.452
65.49	-	-	-	25.45	14.14	1.294	0.044	0.556
67.24	-	-	-	34.52	25.63	1.329	0.048	0.742
69.15	-	-	-	69.94	62.63	1.367	0.051	0.895
72.24	-	-	-	121.42	112.67	1.428	0.056	0.928
74.97	2.37	0.0607	2.309	146.51	129.67	1.482	0.06	0.885
77.77	5.42	0.196	5.224	224.44	190.32	1.537	0.065	0.848
79.62	5.71	0.408	5.302	211.93	165.1	1.574	0.067	0.779
82.42	6.45	0.864	5.586	235.06	165.51	1.629	0.07	0.704
84.44	7.89	1.4	6.49	234.28	151.36	1.669	0.073	0.646
87.31	6.09	2.21	3.88	239.32	145.94	1.725	0.077	0.61

Table 3.2 experimentally measured production cross sections (σ_{expr}), theoretically reproduced cross section (σ_{CF}) and calculated ICF cross section of ^{160}Ho residue along with $\Sigma\sigma_{TF}$, $\Sigma\sigma_{ICF}$, E_{lab}/V_{CB}, V_{rel}/c and F_{ICF} in ^{12}C+^{159}Tb system.

4. ^{12}C+^{181}Ta system

Energy (MeV)	^{186}Ir(α3n)			^{184}Re(2αn)			^{183}Re(2α2n)		
	σ_{expr} (mb)	σ_{CF} (mb) PACE4 K=10	σ_{ICF} (mb)	σ_{expr} (mb)	σ_{CF} (mb) PACE4 K=10	σ_{ICF} (mb)	σ_{expr} (mb)	σ_{CF} (mb) PACE4 K=10	σ_{ICF} (mb)
82.5	43	8.49	34.51	10	-	10	57	0.161	56.84

Table 4.1 experimentally measured production cross sections (σ_{expr}), theoretically reproduced cross section (σ_{CF}) and calculated ICF cross section of ^{186}Ir, ^{184}Re and ^{183}Re residues in ^{12}C+^{181}Ta system.

Energy (MeV)	^{182}Re(2α3n)			$\Sigma\sigma_{TF}$ (mb)	$\Sigma\sigma_{ICF}$ (mb)	E_{lab}/V_{CB}	V_{rel}/c	F_{ICF}
	σ_{expr} (mb)	σ_{CF} (mb) PACE4 K=10	σ_{ICF} (mb)					
82.5	25	0.183	24.817	135	126.16	1.497	0.065	0.93

Table 4.2 experimentally measured production cross sections (σ_{expr}), theoretically reproduced cross section (σ_{CF}) and calculated ICF cross section of ^{182}Re residue along with $\Sigma\sigma_{TF}$, $\Sigma\sigma_{ICF}$, E_{lab}/V_{CB}, V_{rel}/c and F_{ICF} in ^{12}C+^{181}Ta system.

5. ^{16}O+^{130}Te system

Energy (MeV)	^{131}Xe(3α3n)			^{133}Xe(3αn)			^{139}Ce(α3n)		
	σ_{expr} (mb)	σ_{CF} (mb) PACE4 K=10	σ_{ICF} (mb)	σ_{expr} (mb)	σ_{CF} (mb) PACE4 K=10	σ_{ICF} (mb)	σ_{expr} (mb)	σ_{CF} (mb) PACE4 K=10	σ_{ICF} (mb)
61.3	8	-	8	5.1	-	5.1	-	-	-
67.1	12	-	12	30	-	30	107	18.9	88.1
83.2	180	-	180	34	0.0193	33.98	89	22.4	66.6
90.1	320	-	320	80	-	80	183	6.76	176.27

Table 5.1 experimentally measured production cross sections (σ_{expr}), theoretically reproduced cross section (σ_{CF}) and calculated ICF cross section of ^{131}Xe, ^{133}Xe and ^{131}Ce residue in ^{16}O+^{130}Te system.

Energy (MeV)	$\Sigma\sigma_{TF}$ (mb)	$\Sigma\sigma_{ICF}$ (mb)	E_{lab}/V_{CB}	V_{rel}/c	F_{ICF}
61.3	13.1	13.1	1.12	-	1
67.1	149	130.1	1.22	0.027	0.87
83.2	303	280.58	1.52	0.054	0.93
90.11	583	576.27	1.64	0.062	0.99

Table 5.2 $\Sigma\sigma_{TF}$, $\Sigma\sigma_{ICF}$, E_{lab}/V_{CB}, V_{rel}/c and F_{ICF} in $^{16}O+^{130}Te$ system

6. $^{16}O+^{159}Tb$ system

Energy (MeV)	$^{168}Lu(\alpha 3n)$			$^{167}Lu(\alpha 4n)$			$^{166}Tm(\alpha 2n)$		
	σ_{expr} (mb)	σ_{CF} (mb) PACE4 K=10	σ_{ICF} (mb)	σ_{expr} (mb)	σ_{CF} (mb) PACE4 K=10	σ_{ICF} (mb)	σ_{expr} (mb)	σ_{CF} (mb) PACE4 K=10	σ_{ICF} (mb)
75.2	3	3.58	-	-	-	-	-	-	-
78.7	12	13.4	-	-	-	-	1.93	0.0824	1.8476
83.2	57	30.4	26.6	5	1.23	3.77	7	0.113	6.887
87.2	69	40.3	28.7	46	11	35	28	0.0488	27.9512
89.6	87	39.7	47.3	59	23.9	35.1	31	0.0308	30.9692
94.6	145	24.7	120.3	118	62.1	55.9	49	0.0182	48.9818

Table 6.1 experimentally measured production cross sections (σ_{expr}), theoretically reproduced cross section (σ_{CF}) and calculated ICF cross section of ^{168}Lu, ^{167}Lu and ^{166}Tm residues in $^{16}O+^{159}Tb$ system.

Energy (MeV)	$^{167}Yb(\alpha p3n)$			$\Sigma\sigma_{TF}$ (mb)	$\Sigma\sigma_{ICF}$ (mb)	E_{lab}/V_{CB}	V_{rel}/c	F_{ICF}
	σ_{expr} (mb)	σ_{CF} (mb) PACE4 K=10	σ_{ICF} (mb)					
75.2	-	-	-	3	-	-	-	-
78.7	-	-	-	13.93	1.85	1.2	0.03	0.13
83.2	9	0.0451	8.9549	78	46.21	1.27	0.04	0.59
87.2	28	0.237	27.763	171	119.41	1.33	0.045	0.698
89.6	49	0.701	49.299	226	162.67	1.37	0.05	0.72
94.6	21	2.65	118.35	333	243.53	1.44	0.055	0.73

Table 6.2 experimentally measured production cross sections (σ_{expr}), theoretically reproduced cross section (σ_{CF}) and calculated ICF cross section of ^{167}Yb residue along with $\Sigma\sigma_{TF}$,$\Sigma\sigma_{ICF}$, E_{lab}/V_{CB}, V_{rel}/c and F_{ICF} in $^{16}O+^{159}Tb$ system.

7. $^{16}O+^{181}Ta$ system

Energy (MeV)	$^{191}Au(\alpha 2n)$			$^{190}Au(\alpha 3n)$			$^{192}Au(\alpha n)$		
	σ_{expr} (mb)	σ_{CF} (mb) PACE4 K=10	σ_{ICF} (mb)	σ_{expr} (mb)	σ_{CF} (mb) PACE4 K=10	σ_{ICF} (mb)	σ_{expr} (mb)	σ_{CF} (mb) PACE4 K=10	σ_{ICF} (mb)
80	-	-	-	-	-	-	2	0.00171	1.998
85	-	-	-	8	4.2	3.8	10	-	10
87	2	0.3	1.7	6	6.36	-	12	0.00461	11.995
88	2	0.344	1.656	23	6.34	16.66	31	0.00997	30.99
933	3	0.1	2.9	20	7.16	12.84	46	0.114	45.886
97	14	0.0474	13.526	40	4.23	35.77	63	0.363	62.637
99	22	0.00845	21.99	21	3.13	17.87	50	0.338	49.662

Table 7.1 experimentally measured production cross sections (σ_{expr}), theoretically reproduced cross section (σ_{CF}) and calculated ICF cross section of ^{191}Au, ^{190}Au and ^{192}Au residue in $^{16}O+^{181}Ta$ system.

Energy (MeV)	$\Sigma\sigma_{TF}$ (mb)	$\Sigma\sigma_{ICF}$ (mb)	E_{lab}/V_{CB}	V_{rel}/c	F_{ICF}
80	2	1.998	1.12	0.017	0.999
85	18	13.8	1.19	0.031	0.767
87	20	13.695	1.22	0.035	0.685
88	56	49.306	1.23	0.037	0.88
93	69	61.626	1.30	0.045	0.893
97	117	111.933	1.36	0.05	0.957
99	93	89.522	1.39	0.053	0.963

Table 7.2 $\Sigma\sigma_{TF}$, $\Sigma\sigma_{ICF}$, E_{lab}/V_{CB}, V_{rel}/c and F_{ICF} in $^{16}O+^{181}Ta$ system.